Drug Dynamics Study in the Ionic-liquid Environment using PFG-Diffusion, Relaxation NMR and Computational Calculations

Raj Kumar

(MS15049)

A dissertation submitted for the partial fulfillment of

BS-MS dual degree in Science

Indian Institute of Science Education and Research Mohali

May 2020

Certificate of Examination

This is to certify that the dissertation titled " **Drug Dynamics Study in the Ionic-liquid Environment using PFG-Diffusion, Relaxation NMR and Computational Calculations**" submitted by Mr. Raj Kumar (Reg. No. MS15049) for the partial fulfillment of BS-MS dual degree programme of the institute, has been examined by the thesis committee duly appointed by the institute. The committee finds the work done by the candidate satisfactory and recommends that the report be accepted.

Prof. Arvind Dr. Sugumar Venkataramani Prof. Kavita Dorai

(Supervisor)

Dated: June 05, 2020

Declaration

The work presented in this dissertation has been carried out by me under the guidance of **Prof. Kavita Dorai** at the Indian Institute of Science Education and Research, Mohali.

This work has not been submitted in part or in full for a degree, a diploma, or a fellowship to any other university or institute. Whenever contributions of others are involved, every effort is made to indicate this clearly, with due acknowledgement of collaborative research and discussions. This thesis is a bonafide record of original work done by me and all sources listed within have been detailed in the bibliography.

Raj Kumar

(Candidate)

June 05, 2020

In my capacity as the supervisor of the candidate's project work, I certify that the above statements by the candidate are true to the best of my knowledge.

Prof. Kavita Dorai

(Thesis supervisor)

Acknowledgement

I am genuinely grateful to my supervisor Prof. Kavita Dorai for her constant support & guidance throughout the thesis period. Her positive and calm disposition in every situation is something I would like to imbibe. The discussions I had with her have enhanced my capabilities as a researcher. She truly is a great mentor. I could not have imagined having a better advisor and mentor for my Master's thesis. Besides my supervisor, I thank the rest of my thesis committee members, Prof. Arvind and Dr. Sugumar Venkataramani. .

Periodic discussions with Rakesh Sharma and Jyotsana Ojha have been a big help throughout the thesis work for which I am thankful to them. Their expertise in Relaxation and Diffusion NMR has been very helpful for my understanding of the topic. I would like to mention my special thanks to my senior and scientific assistant of NMR lab- Balvir singh, Sumit Mishra, Dileep singh, and Akshay Gaikwad, Akansha Gautam and Vaishali Gulati for their continuous support and availability for discussion all the time, and it always helped me to get new insights into my work.

I would also like to acknowledge my friend Zinnia Arora's inquisitive inquiries on my thesis topic which have helped me articulate my views on these topics better. It would be remiss of me to forget to thank my family and friends for maintaining sufficient peace and health in their life so that I don't have to be overly-bothered about them. Generic discussions with Rohit Negi and Amit Kumar have been a great source of amusement throughout the thesis period. I would like to thank my friends Saurabh Bedi, Vaibhav Pal and Surendra Yadav, They have been there to help me whenever needed. I would like to thank all of them for making my stay at IISER Mohali a memorable one.

I express my immense gratitude to all faculties and students of IISER Mohali for providing me access to research facilities. I duly acknowledge the financial support from DST-INSPIRE Scholarship to pursue BS-MS at IISER Mohali.

I owe my deepest gratitude to my parents and my siblings for their blessings, faith and sacrifices. Their support has always strengthened and inspired me, and they have been the strongest sources of support, guidance, and motivation to me.

Raj Kumar

List of Figures

List of Tables

Contents

MOTIVATION

It is experimentally reported that 1-butyl-3-methylimidazolium bromide [BMIM] [Br], IL and D_20 micro emulsion system, can be used in the transdermal delivery of a poorly permeating drug 5-Furacil.

Results of *ex vivo* skin permeation studies through mice's skin showed that the selected IL/water Microemulsion exhibited 4-fold enhancement in the percent of drug permeation and 2.6 fold enhancement in solubility compared to the aqueous solution. Drug+IL micro emulsion successfully treated skin tumors in 4 weeks. In contrast, conventional ointment (C_2) and the commercial cream (C_4) were ineffective in regaining the physiology of skin after four weeks of the treatment period. Besides, the side effects like erythema and irritation allied with the traditional formulations were not witnessed.

Ionic liquids have the potential to disrupt bacterial cell membranes and enhance the delivery of antibiotics through the outer layer of skin that can help in tackling with antibiotic-resistant germs. Biofilm-protected bacteria cause around 80% of resistant. Ionic liquid's broad range of properties can help to develop medicines that can so speak help “to fight fire with fire”, means toxicity of IL can be fine-tuned to maintain the level of toxicity that will achieve the task of killing malignant cells.

Such studies give confidence that the application of the IL-based ME system can help in enhancing the permeability, solubility, and therapeutic potency of 5-Furacil. Hence, the study of drug - IL interaction can help in revealing the factors which are causing such stability. It will also be useful for further improvement in its solubility, permeability, and bioavailability for skin cancer treatment.

ABSTRACT

The pharma industries are facing many challenges in the drug delivery of newly discovered drug molecules due to their low bioavailability, solubility, polymorphic conversion, and stability. Such limitations further got intensified if a drug is partially soluble or insoluble in water or any other pharmaceutically approved organic solvents. In the pharmaceutical sciences, innovation is needed to overcome these barriers for the formulation of drugs and systems for efficient drug delivery.

In this work, we focused on investigating the dissolution mechanism and hydrogen-bonding interactions between 5-Fluorouracil (A pyrimidine nucleic acid-base) and IL, 1-Butyl-3-methylimidazolium bromide using the combined application of ^{19}F, ^{1}H NMR, and $^{1}H-^{1}H$ NOESY NMR spectroscopy along with quantum chemical calculations using Gaussian 09.

The bifunctional dissolution nature of IL can be deduced via the presence of interactions between both ions of the $[BMIM]^{+}$ $[Br]^{-}$ and 5-Furacil that is responsible for the dissolution mechanism, which involves hydrogen bonding between the drug-cation and anion of IL. The location of these interaction sites is attempted to unveil using the relaxation and diffusion NMR experiments, complemented by Gaussian calculations, which provided additional evidence concerning the cation-5-Furacil interactions.

CHAPTER-1

Introduction to NMR Spectroscopy

1.1 Introduction

From a simply savvy perspective, an entrancing aspect concerning nuclear magnetic resonance (NMR) is the unpredictability of the subject. In any case, this intricacy can be the wellspring of much disappointment for those wishing to comprehend and utilize NMR. Similarly, as with other physical strategies utilized in investigations of organic frameworks, NMR might be utilized in an exact mode, for instance, essentially taking note of varieties in an NMR parameter with modification of a trial variable. Be that as it may, a superior comprehension of the NMR wonder is frequently remunerated with extra clarification of the framework under examination. Despite the fact that there might be limits of information on NMR important to peruse the writing fundamentally or to lead NMR examines, there is a continuum of information to be increased about NMR that has the down to earth profit of empowering an ever more prominent assortment of NMR experiments to be used accurately. The sight of nuclear magnetic resonance can be easily expressed in essence, as given below. In NMR, the sample of a compound is placed in a magnetized field with providing suitable frequency; radio frequency is needed in NMR. By this absorption of energy is done by the sample, the radiation frequency for suitable absorption energy mainly subject to two different things. First, the type of nucleus is one of its major Characteristic (e.g., ^{1}H, ^{13}C or ^{19}F or). Second, the chemical environment of the present nucleus that affects the frequency.

1.2 Basics of NMR Spectroscopy

Spectroscopy can be defined as the study of the interaction of light with matter. It's the fundamental exploratory tool in the field of science that allows the investigation of the composition and structure of matter at the molecular scale, microscale, and astronomical distance. In particular, NMR is a technique that depends on the spin, an intrinsic property of every nucleus, where spins are exposed to a constant and strong magnetic field. After

that, these spins are excited by a radiofrequency pulse sequence. The spin precession is noted during the free induction decay of the nuclear magnetic resonance experiment and transformed into a frequency domain spectrum after Fourier transformation.

It is a strategy that depends on the inherent turn properties of cores. In which twists are first presented to a solid and consistent attractive field. At that point, they are energized by a radio recurrence beat arrangement. The pre-session of the twists is noted during the free acceptance root of the nuclear magnetic resonance try and changed over in a recurrence range after Fourier change. Atomic attractive reverberation spectroscopy is hypothetically a fantastic instrument for fair-minded metabolic profiling of all little particle metabolites since the strategy depends on the detection of any atoms that contain carbon or hydrogen. [1, 2]

1.3 Magnetic Resonance

1.3.1 Nuclear Spin

Positive charge is occupied by every nuclei. Numerous nuclei carry on as if they are turning. Anything in that environment that is charged and moves have an attractive magnetic moment and generate an attractive magnetic field. Accordingly, a turning nucleus goes about as a minor bar magnet situated in the direction of spin revolution axis. Nuclear spin is the name given to regularly small magnet. On the off chance, we place this little magnet in the area (field) of a lot bigger magnet, its direction will never again be irregular. Most likely, there will be one direction. Notwithstanding, if the modest magnet is situated unequivocally 180˚ the other way, that position could likewise be kept up (take few magnets and play with them to test this). In scientific vocabulary, the most ideal alignment would be the lower energy state and the less preferred direction. Two-state description is exact for almost all nuclei of biological interest ^{1}H, ^{15}N, ^{13}C, ^{31}P, ^{19}F, etc. It is a quantum approaches that nucleus with nuclear spin (I= ½) be in the two-states when the nuclei are placed in an attractive magnetic field. Most common isotopes of carbon, oxygen, nitrogen are NMR inactive.

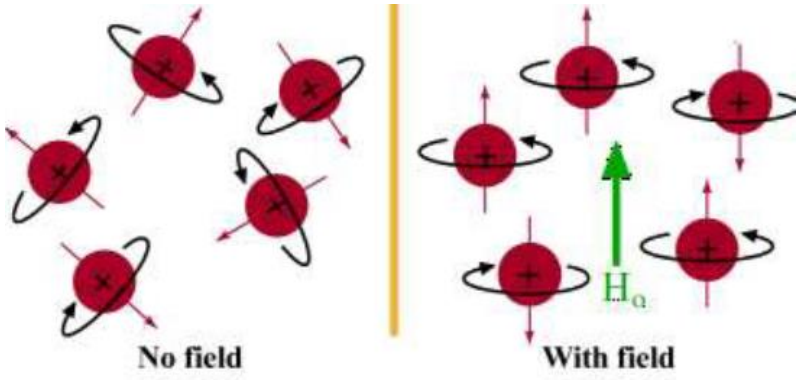

Figure 1.1: Alignment of nuclear spins in the absence and presence of external Magnetic field. [3]

1.3.2 The Splitting of Energy levels in Magnetic field (Zeeman splitting)

Quantum mechanics reveals to that a nucleus of nuclear spin I will have *(2I + 1)* potential directions or possible alignment. Any nuclei with I = 1/2 value will have two possible directions. Without an outer (magnetic) attractive field, these directions are of equivalent vitality (energy). On the off chance that an attractive field is applied, at that point the energy levels split that is known as Zeeman splitting. Each level is given a quantum number that is denoted by (m) and known as magnetic quantum number.

Boltzmann distribution determines the energy level of initial population when the nucleus is opened up in the attractive (magnetic) field. Boltzmann distribution explains the more nuclei presents within the lower energy-levels as compared to higher energy-levels. With electromagnetic radiations, it is easy to excite the lower level nuclei to higher energy level. Difference in energy across the levels will determine the radiation frequency. The formula that exactly explain the difference of energy is

$$\Delta E = h\nu_0 = \frac{h\gamma B_0}{2\pi}$$

Here, γ is the gyromagnetic ratio & applied magnetic field is denoted by B_0.

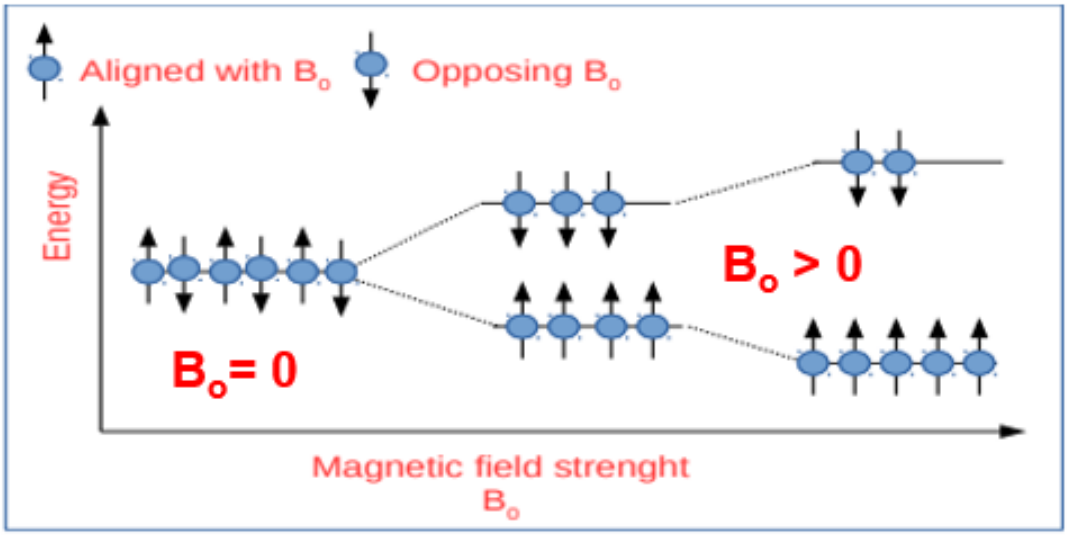

Figure 1.2: Energy level Splitting in magnetic field for a nucleus with spin quantum no, *I= 1/2*. [4]

A frequency which is used in precessional motion is known as Larmour frequency. In the scenario, when a proton is set in an attractive (magnetic) field, it will attempt to adjust itself toward the applied magnetic field. The spins either adjusted toward the path (lower energy levels) of applied field or the other way (higher energy levels). As clarified by Boltzmann the lower energy level will contain marginally a bigger number of nuclei than the more significant level that will create net charge along the z-axis (only if this applied attractive field is along the Z-axis). In the event that the charge isn't adjusted accurately with the applied magnetic field, at that point this prompts a precessional movement of net polarization around the Z-axis. [5, 6] The precise recurrence of this precessional movement is known as Larmour recurrence or frequency and is given by

$$\omega_0 = -\gamma B_0$$

Here $B_\circ$ is external applied magnetic field.

1.3.3 Magnetisation

The above portrayal of nuclear polarization depends basically on quantum mechanics. In any case, another method for review the NMR wonder is to utilize an old style mechanical portrayal. For a nuclear spin I = ½, in magnetic field of solidarity B_o, the

magnetic moment of nuclei will process about the Z-axis characterized by the bearing of the attractive field.[7]

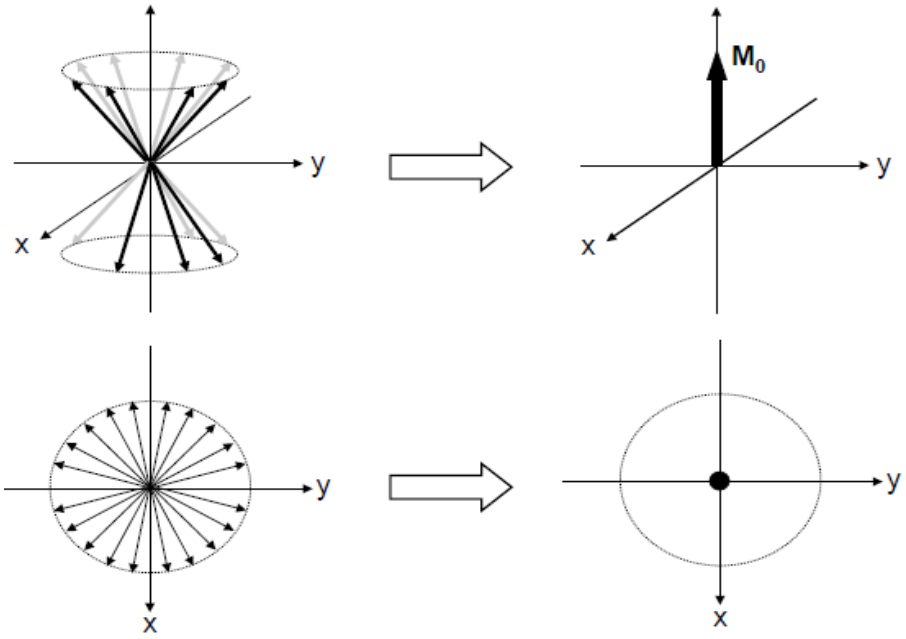

Figure 1.3: Precession and orientation of nuclear spins at thermal equilibrium in a constant magnetic field ($B_{0)}$ along the Z-axis.

In a good example, we will have countless nuclear twists all precessing around the z-pivot (z-axis). That is appeared in the above (figure 1.3) yet with a substantially more flexible number of nuclear arrows. This conversation realizes that the alignment of nuclei will either be parallel or antiparallel in the presence of the attractive magnetic field. Subsequently, a few spins precess about the positive z-pivot and some negative z-pivot. The polarization radiating from a genuine source is essentially the whole set of all the individual nuclear magnetic moments (spin). We are probably aware of the past conversation. There will be a small overabundance of nuclei situated within the attractive field, for example, in the low energy (vitality) level. Therefore the total will generate a net magnetisation charge in the direction of +z-pivot; this will be the absolute charge that decides an NMR signal, not the interacting magnetic moment of each nuclei alone.

Generally, we use Fourier Transform Nuclear magnetic resonance for typical many different nuclei. However, FID is a time domain signal. The common frequency domain

spectra could be easily got by doing the Fourier transformation of the averaged signal free induction decay (FID).

1.4 Nuclear Magnetic Resonance parameters for Interaction

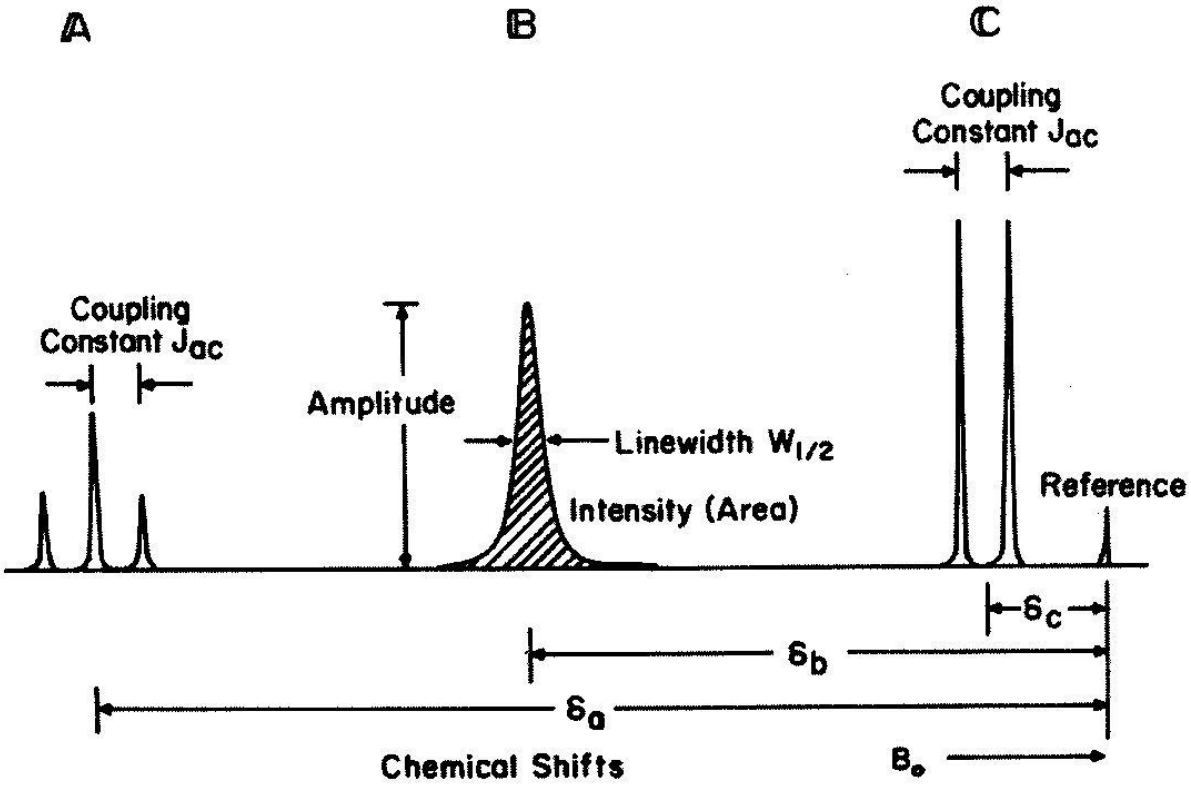

Figure 1.4: 1D Nuclear magnetic resonance spectral parameters [8]

The different NMR otherworldly parameters to be talked about in this way are shown above.

1.4.1 Chemical Shift

The frequency dispersion in the NMR signals of nuclei occurs due to the difference in the electronic environment envelope the nuclei. The torque produced by the interactive static field likewise causes electrons' precession around the attractive static field. The directional electric precession creates a neighborhood interactive field with greatness corresponding to $B_{\circ}$, which

shields a part of a similar static field from the nuclei. The net effect is described by the shielding constant σ

$$\nu = \frac{\gamma}{2\pi} B_0(1-\sigma) = \frac{\gamma}{2\pi} B_1$$

Where $B_1 = B_\circ\ (1-\sigma\ )$ is the magnetic field felt by each spin. since the chemical shift and larmour recurrence are both relative to the applied interactive-magnetic field (B_0), the proportion of these two quantities will be fixed, thus it is advantageous to communicate chemical shift as far as this proportion as then it won't be magnetic field dependent. The field-independent expression for the chemical shift is

$$\delta = \frac{\omega^\circ - \omega^\circ_{ref}}{\omega^\circ_{ref}}$$

Where ω° is the larmour frequency of a particular nucleus and ω°_{ref} is a larmour frequency of the same isotope of the reference compound within the same attractive (magnetic) field. If in the event that the quality of static attractive field is expanded, at that point the two amounts ω° and ω°_{ref} increase in the equivalent ratio, so that δ stay consistent. The estimation of chemical shift is exceptionally small hence it has been multiplied by 10^6 and afterward cited as parts per million (ppm).

The value of δ always increase from right to left by convention in the spectra. The accompanying properties: a) an unaltered concoction move an incentive over a large scope of temperature and pH esteems, b) steadiness in an assortment of solvents, and c) case of handling, are required to have in the reference compound. Two compounds are generally used for ^1H NMR reference: 2,2-dimethyl-2-silapentane-5-sulfonic acid (DSS)[HBS^+01 and tetramethyl-silane (TMS)].

1.4.2 Line width: The connection between the base line width $W_{1/2}$ and T_2 unwinding has just been given as

$$W_{1/2} = 1/(\pi T_2)$$

In tests with macromolecules the line width might be more extensive as compared to the scalar splitting, that's why the last one may not really be clear. It ought to likewise be noticed that quickly exchanging –NH and -OH protons (vide infra) don't cause splitting.

In any case, if coupling constants (J) can be resolved, now they can again uncover insights regarding molecular geometry.

1.4.3 Spin-spin coupling (J coupling)

Spin-spin coupling (likewise called J coupling or scalar coupling) is the impact on nuclear spin (*A)* brought about by the nearby interactive field generated by its neighbour spin (*B)*. The direction alignment of spin *B* in the interactive magnetic field creates a little polarization of the electrons for the most part in the s-orbital surrounding spin *B*. The electron distribution density of spin (*A)* legitimately attached to spin *B* influences with this polarization. Since the association depends on the s-orbital electron density at the pair of nuclei, the nuclei's electron density must be related. Subsequently, J coupling engenders just along with synthetic or chemical bonds. Despite the anisotropic nature of J coupling, which is because of the asymmetric environment encompassing the nuclear spin, the cooperation is found in the middle value of an isotropic incentive in the arrangement by the fast molecular tumbling motion. The J coupling magnitude lessens fundamentally as the number of bonds isolating the nuclei increments. Two and three bond couplings are at least one magnitude weaker than one-bond J couplings. Whereas couplings more than three bonds are near zero, with an exemption that long-extend coupling past three bonds is detectable in double bonded compounds.

1.4.4 Dipolar Coupling:

The dipolar contribution for weakly coupled spins to the observed resonance is given by

$$\nu_D = \nu_{||}\frac{3Cos^2\theta-1}{2}$$

Where θ an angle between the magnetic field and dipole vector and $\nu_{||}$ is the magnitude of dipole vector.

$$\nu_{||} = -\frac{\gamma_1\gamma_2 h}{4\pi^2 r^3}$$

Where r represents the separation between spins 1, and 2 that has the gyromagnetic proportions of γ_1, and γ_2 respectively. The dipolar collaboration between two nuclear spin happens through space. The dipolar coupling steady decrease with the expansion of the Dipole-Dipole (DD) separation as a function of separation distance (r^{-3}). In the solution, dipolar splitting isn't discernible in light of the fact that the orientation term of the dipolar collaboration as for the attractive magnetic field heading is arrived at the midpoint of to zero by fast molecular tumbling. Be that as it may, the impact of dipolar connection on molecular relaxation still exists, that is the starting point of the Nuclear overhouser effect (NOE).

1.4.5 NUCLEAR OVERHOUSER EFFECT

The Nuclear Over Houser effect (NOE) is an unwinding parameter that has been utilized as an essential instrument for deciding (3-D) three-dimensional sub-atomic structures. At the point where two-nuclei are inadequately close to spatial nearness, here might have cooperation in the two dipole moments. The interaction between an attractive field and a nuclear dipole moment produced by another was at that point that is noted to give an instrument to relaxation. The atomic dipole-dipole coupling subsequently prompts the NOE just as T1 relaxation. On the off chance that there is any instrument other than atomic dipole-dipole associations that prompt relaxation, from an unpaired-electron, the Nuclear Overhouser effect will be lessened or may demolish.

1.5 Quantum Mechanical Description of Nuclei in static and oscillating field

The Schrodinger equation's description in elementary quantum mechanics is given as-

$$i\hbar \frac{d|\psi>}{dt} = \hat{H}(t)|\psi>$$

For the case in which Hamiltonian is time-independent, then the solution will be

$$|\psi(t)\rangle = e^{\left(\frac{-i\hat{H}t}{\hbar}\right)}|\psi(0)\rangle$$

If $\hat{H}$ is time-dependent, then the solution is given by

$$|\psi(t)\rangle = e^{\left(\int -\frac{i\hat{H}(t)dt}{\hbar}\right)}|\psi(0)\rangle$$

In the case of NMR, Usually, we work upon the time-dependent Hamiltonian. That's why it's preferred a bit convenient to write the hamiltonian in a different frame of reference to cancel out its time dependency. There are two different frames of references, which we will understand to get time-independent Hamiltonian. [9, 10].

1.5.1 Interaction frame

Generally, the total Hamiltonian of a quantum system can be written as the linear combination of the two Hamiltonians in which one component is relatively much larger than the second one ($\hat{H}_0 >> \hat{H}_1$).

The system could be written as;

$$\hat{H}_{\text{total}} = \hat{H}_0 + \hat{H}_1$$

To get a better understanding of the dynamics of the system in the presence of $\hat{H}_1$ alone, let's define a new state

$$|\emptyset(t)\rangle = e^{\left(\frac{i\hat{H}t}{\hbar}\right)}|\psi(t)\rangle$$

By differentiating the above equation, we get

$$\frac{d|\emptyset(t)\rangle}{dt} = \frac{i}{\hbar}\hat{H}_0 e^{\left(\frac{i\hat{H}_o t}{\hbar}\right)}|\psi(t)\rangle + e^{\left(\frac{i\hat{H}_o t}{\hbar}\right)}\frac{d|\psi(t)\rangle}{dt}$$

Then we multiply it by $i\hbar$ from both side and by further solving, we get

$$i\hbar\frac{d|\emptyset(t)\rangle}{dt} = \hat{H}'_1|\emptyset(t)\rangle$$

1.5.2 Rotating frame

For a single-spin external Hamiltonian can be written as:

$$\hat{H}_{\text{lab}} = \hat{H}_{\text{Zeeman}} + \hat{H}_{\text{r f}}$$

$$\hat{H}_{lab} = - \hbar\omega_o\hat{i}_z - \hbar\omega_1 [\hat{I}_x\cos(w_{rf}t) + \hat{I}_y\sin(w_{rf}t)]$$

By combining above equation by using rotation-sandwich relations as

$$\hat{H}_{lab} = - \hbar[e^{-\nu w_r t}(\omega_o\hat{I}_z + \omega^1\hat{I}_x)\, e^{\nu w_r t}]$$

Then by transforming the new state by following rule as

$$|\psi'(t)\rangle = e^{w_{ro}t\hat{I}}|\psi(t)\rangle$$

The dynamics of the rule is given by

$$i\hbar\frac{d|\psi'(t)\rangle}{dt} = \hat{H}'|\psi'(t)\rangle$$

Where effective Hamiltonian is given as $\hat{H}$

$$\hat{H} = \hbar(\omega_o - \omega rot)\hat{I}_z - \omega^1\hbar\,\hat{I}_x$$

Consequently, $\omega_o = \omega_{rot}$ this is called on resonance condition and as a result magnetisation in the rotating frame will be along the x-direction.

1.6 Fourier Transformation and Acquisition of NMR Spectrum

The electric oscillating current induced with the processing of nuclear transverse magnetization is referred as Free Induction decay (FID). It is the time domain signal which is digitized and then fourier transformed to get a frequency spectrum of the NMR signals.

The Fourier transformation (FT) describe the correlation between two functions by dependent variables, like- frequency and time, called a Fourier pair relationship.

$$F(\omega) = Ft\big(f(t)\big) = \int_{-\infty}^{\infty} f(t)e^{-i\omega t}\,dt$$

& the inverse of FT can be obtained as follow-

$$f(t) = Ft\big(F(\omega)\big) = \int_{-\infty}^{\infty} F(\omega) e^{i\omega t}\, d\omega$$

In the case NMR signal defined as an exponential function along with a decay constant of 1/T:

$$f(t) = e^{\left(i\omega^{\circ} - \frac{1}{T}\right)t}$$

The Fourier Transformation will have the form:

$$F(\omega) = Ft\big(f(t)\big) = \int_{-\infty}^{\infty} f(t) e^{\left(i\omega^{\circ} - \frac{1}{T}\right)} e^{-i\omega t}\, dt = \frac{i(\omega^{\circ} - \omega) + \left(\frac{1}{T}\right)}{(\omega^{\circ} - \omega)^2 + \frac{1}{T)^2}}$$

This form indicates the frequency signal follow Lorentzian line shape. NMR spectra from FIDs is generally obtain from the cooley fat fourier transformation algorithm combined with techniques like maximum entropy [SSB^{+}84, MDKL89, SH92] and linear prediction [ZB90, BdBBvO85].

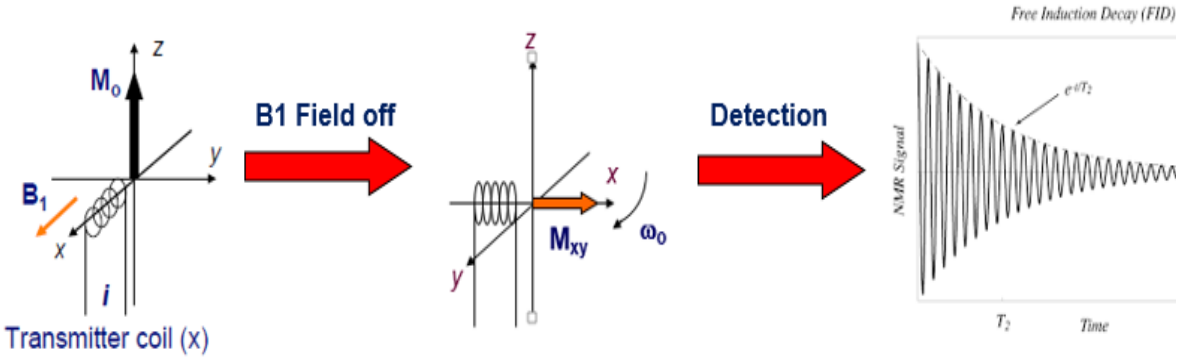

Figure 1.5: Pictorial depiction of acquisition and detection of NMR spectrum

To excite the transitions by covering all possible frequency regions, the bandwidth of excitation is needed to be sufficiently large, that can be obtained by applying short radio frequency pulses. For selective excitation, the bandwidth of excitation needs to be relatively narrow in order to excite a small range of Resonance frequencies (RF). The

short pulse durations are within few microseconds that are sometimes known as hard pulses; on the other side, the long pulses may last up to hundreds of milliseconds and referred to as soft pulses. The short pulse bandwidth may cover numerous kilohertz, and t long pulses selectivity can be narrowed down up to a few hertz. The Fourier transformation of short, and long rectangular shape pulses are given below-

$$\mathrm{rect}\frac{\mathrm{t}-\mathrm{X}}{\mathrm{Y}} = \mathrm{u}\left(\mathrm{t}-\mathrm{X}+\frac{\mathrm{Y}}{2}\right) - \mathrm{u}\left(\mathrm{t}-\mathrm{X}-\frac{\mathrm{Y}}{2}\right)$$

This mathematical function is centered about *X* and *Y* is duration here. This rectangular function is a special case of boxcar function. It gives zero value throughout the real line except, for a single interval in which domain it gives some constant value-

$$F(\omega) = \int_{-\infty}^{\infty} rect(t)e^{-i\omega t}\,dt = \mathrm{sinc}\frac{\omega}{2\pi}$$

During the analog to digital conversion of the NMR signals, the analog NMR signal is acquired/ sampled with a particular sampling rate by the device ADC, which is used for the conversion of NMR signal from a voltage to binary code. The Nyquist theorem states that to accurately represent the frequency values, the sampling rate is necessary to be minimally double of the highest frequency value.

Chapter 2

Relaxation and PFG- Diffusion NMR

2.1 Introduction

Relaxation NMR phenomena is based on the excitation of a system of nuclear magnetic moments and further, its relaxation or returning to the equilibrium state. The relaxation time parameter, such as T_1, T_2, and NOEs, can contribute to reveal relevant information related to the molecular dynamics of the molecules in the solution state.

Diffusion is the random/ stochastic translational movement of ions or molecules driven by the system's internal energy; it's the basic mechanism by which molecules can rearrange themselves after perturbing the system. It's a very elemental form of transport in the chemical and biophysical systems. Therefore, to get the intuition about the translational diffusion coefficient can be useful to understand the governing process, constituents, and system dynamics.

2.2 Relaxation

Nuclear spin relaxation is a mind-boggling phenomenon that is firmly associated with the molecular movements and separation parameters that are typically challenging to extricate from the information given by the relaxation process. Dipole-dipole collaboration is the most significant relaxation system for some nuclei with the spin ($I = 1/2$), which is simply an interaction through-space. Another significant association promoting nuclear relaxation is chemical shift anisotropy (CSA), which can interact through-bond and through-space. In the case of quadrupolar nuclei ($I \geq 1$). The relaxation is typically overwhelmed by the quadrupolar relaxation mechanism. This fast relaxation creates broad and uncertain lines for the quadrupolar nucleus. An excellent case to show the use of relaxation data to gain insight into the structure and dynamics of a strong/ hard material has been published. [11] An examination of the temperature reliance of

deuterium and carbon spin-lattice relaxation rates made it conceivable to distinguish a fundamental mechanism by adding to the relaxation of nuclei and proposing a molecular model reorientation in solid materials.

The most common and contemplated relaxation process is homo-nuclear ^{1}H-^{1}H DD cross-relaxation in natural particles, molecules, and bio-macromolecules, known as the Nuclear-over hauser (NOE) impact, by this method data on inter-nuclear separations can be collected. The cross-relaxation rate relies upon $1/r^{6}$, where r is the inter-nuclear separation distance; this is broadly being used to gauge distances via cross-relaxation experiments. Notwithstanding, the communicating spins are infrequently disconnected from the interactions with other spins, the subsequent spin dispersion confuses the quantitative translation of the NOE-type operations. Nonetheless, a semi-quantitative separation estimation is typically adequate for the assurance of the compliance and relative arrangement of biological, and organic molecules.

Spin relaxation rates are upgraded within the insight of para-magnetic focuses on the samples. Nuclear relaxation could be utilized, for instance, to restrict the metal ion inside the protein framework. [12] Paramagnetic relaxation based imperatives can be dealt with correspondingly to typical NOE inferable from the r^{-6} reliance of paramagnetic-relaxation improvement. A significant characteristic of the paramagnetic relaxation is that they have long range; it's because the electron's magnetic moment is around (658) multiple times bigger than that of the ^{1}H.

Classification of Relaxation Phenomena-

Phenomenologically, the relaxation process can be categorized into two types:

2.2.1 Longitudinal Relaxation (T_1):

At equilibrium, the net alignment of spins is along (+Z) direction. When we apply 180 R.F. pulse, it disturbs the magnetization and brings in (-Z) direction.

The rate at which the z-component of longitudinal magnetization returns to its equilibrium state is characterized by a time constant T_1 that is called longitudinal relaxation. It is an enthalpic process in which energy is taken or transferred from other

spin systems to the surrounding. The surrounding of spins is referred to as lattice, and therefore T_1 value is usually called the spin-lattice relaxation time.

2.2.2 Measurement of T_1 (Inversion recovery experiment)

There are many distinct methods that can be utilized to measure T_1 relaxation. Commonly used (and more accurate the best) method to measure T_1 is to apply the inversion recovery pulse sequence ($\pi - \tau - \pi/2$).

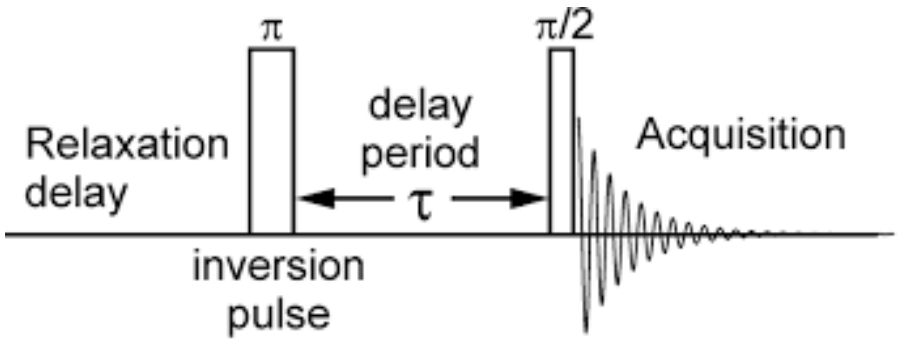

Figure 2.1: Schematic showing of the inversion recovery Pulse sequence. [13]

In order to measure T_1, the equilibrium magnetization (+z magnetization, M_{zo}) is first inverted by applying a π pulse that creates -z magnetization ($-M_{zo}$), the spin system begins relaxing toward thermal equilibrium (M_{zo}). Relaxation with time τ occurs according to the following equation:

$$M_Z(\tau) = M_{ZO}\left(1 - 2\exp\left(-\frac{\tau}{T_1}\right)\right)$$

After time interval τ, a $\pi/2$ pulse got applied, and the Free induction decay (FID) just after the pulse is acquired. This 90° pulse brings the net magnetisation into xy-plane, which is necessary to detect any magnetization because signal detection is possible only in the xy or transverse plane. As τ becomes larger, this magnetisation approaches the equilibrium population distribution even more closely, as can be seen in the figure below.

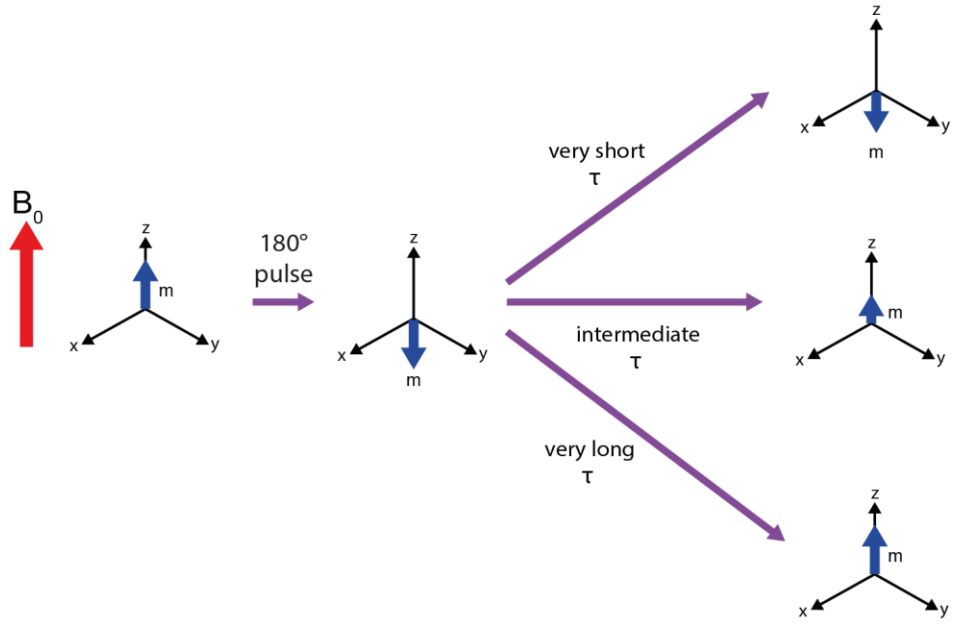

Figure 2.2: A graphic representation of change in bulk magnetization with varying delays and pulses. [14]

As shown in figure 2.2, after applying the pulse, the signal is 1st inverted and once the delay between the pulses is long enough the magnetization becomes positive.

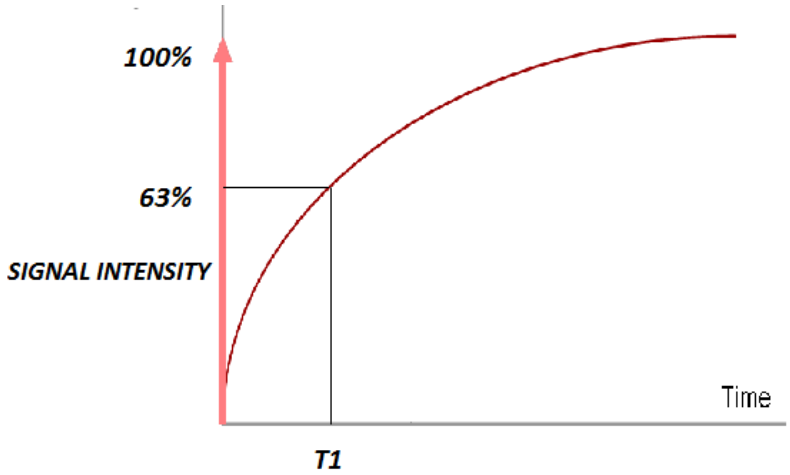

Figure 2.3: A graph of the intensity vs the relaxation delay, showing the recovery of magnetisation along +Z axis. [15]

It can easily be verified from the equation that at $\tau = 0$ (immediately after the πpulse), $M_z(0) = -M_z(0)$, and as $\tau \rightarrow$infinity, $M_z(\infty) \rightarrow +M_z(0)$.

2.2.3 Transverse Relaxation (T_2 relaxation)

Applying 90^0 R.F. pulse at equilibrium brings the +z magnetization into the xy plane. Then, this net magnetization starts decaying in the xy plane. The rate at which xy-magnetization decays to zero is characterized by a time constant T_2 that is called transverse relaxation that defines the decay rate of magnetization in the transverse (xy) plane. Analogously, the similar time constant is referred to as T_2.

The transverse relaxation is a measure of how rapidly the phase coherence among nuclear spins decays. Consequently, this dephasing in the nuclear spins does not provoke any variations in the comparative population of both the +1/2 and -1/2 state. So, it will not change the net energy of the spin system of interest. Transverse relaxation is solely an entropic process, sometimes known as spin - spin relaxation.

2.2.4 Measurement of T_2: Carr-Purcell-Meiboom-Gill (CPMG) Sequence

Measurement of transverse relaxation time (T_2) is mostly carried out utilizing, Carr Purcell pulse sequence combined with the modification of Meiboom-Gill.

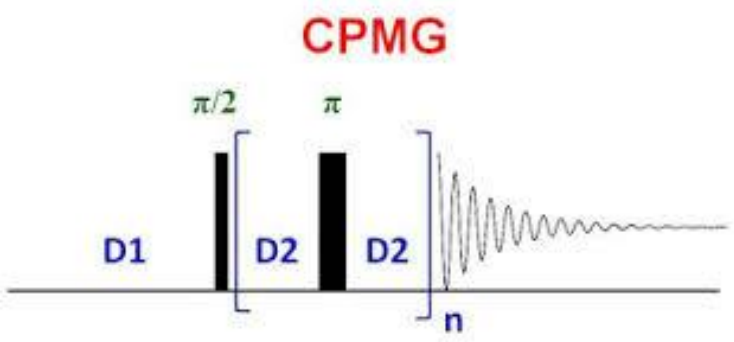

Figure 2.4: Schematic showing of the Carr-Purcell-Meiboom-Gill (CPMG) Sequence. [16]

A π/2 pulse brings the equilibrium magnetisation in the xy-plane. As the magnetic field (Bo) is not entirely uniform, so each magnetic spins will feel a bit different precessional/rotational frequencies. As a result, the individual nuclear spins will fan out in the xy-plane with a loss of phase coherence. Following a time delay, a π pulse is applied, as the processional frequencies of the individual spins are still the same in the opposite direction than the previous one; they will achieve the phase coherence at time 2 τ along the negative y axis. This phenomenon will appear in a signal called spin echo, which will be detected. After the spin echo, spins will again fan out, and phase coherence will be lost, which can be regained by applying another one π pulse

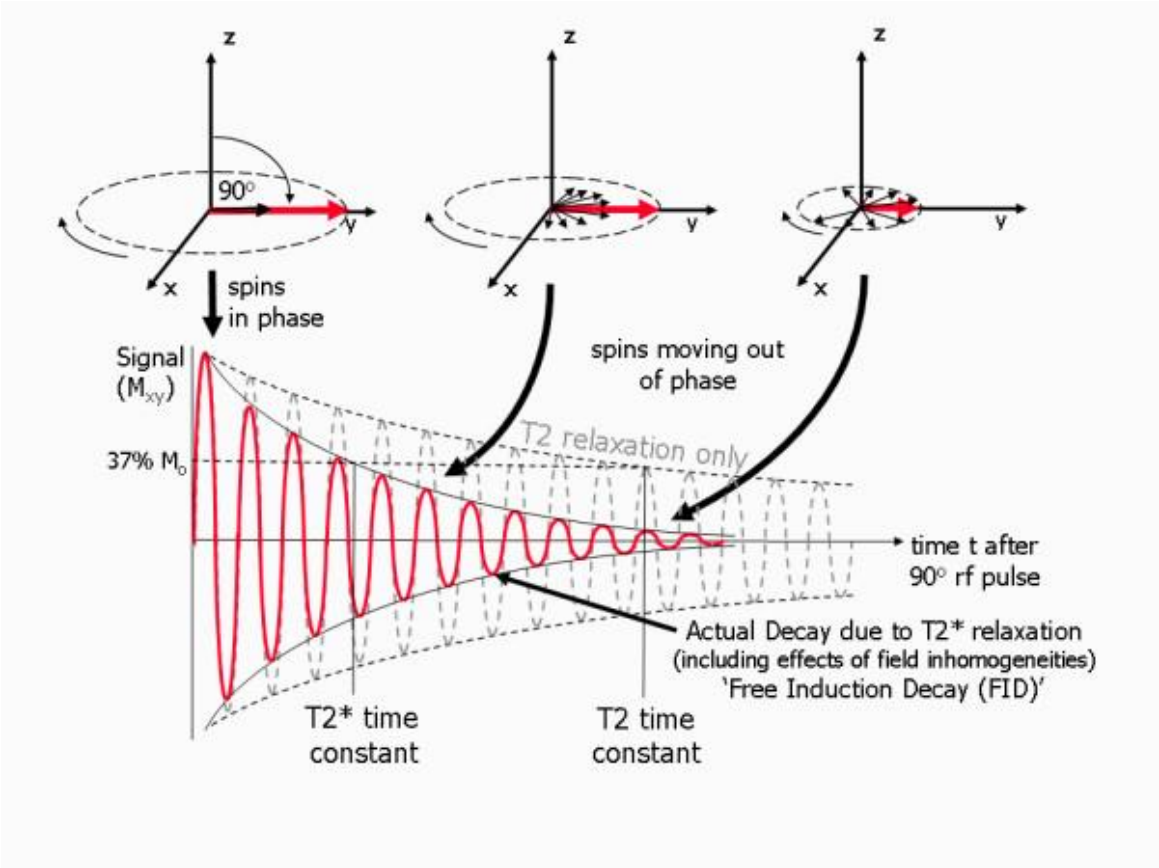

Figure 2.4: A graphic depiction of how the bulk magnetization changes in transverse relaxation experiment and a plot of the intensity vs the delay times. [17]

The CPMG sequence starts with a 90^0 pulse followed by a series of 180^0 pulse. It is a train of spin-echoes signals which follow each and every π pulse exactly in the midway of another π pulse. The decay in magnitudes of the echoes follow the exponential trend as the train of echoes proceeds, and this decay in echo magnitude (T_2) occur according to the following equation:

$$M_{xy}(\tau) = M_o \exp(-\frac{\tau}{T_2})$$

In the written equation, where τ is the time duration from the $\pi/2$ pulse to the top of an echo. Finally, T_2 can be calculated by recording the spectrum at different values for τ and fitting the data in the above equation.

It is easy to verify from this equation that at $\tau = 0$ (immediately after the π/2 pulse), $M_{xy}(0) = M_{zo}$, and as $\tau \rightarrow \infty$, $M_{xy}(\infty) \rightarrow 0$.

2.2.5 Causes of Relaxation

In the case of spin-1/2 nuclei, the relaxation processes take place through the interaction of magnetic fields produced by magnetic dipoles with the nuclear spin. This applied magnetic field fluctuates due to random molecular motions, both translational and rotational. The relaxation times T_1 and T_2 depends on the rate of molecular motion and the nature of the molecule.

Molecular motions which take place at a rate close to the resonance frequency (RF) for the nuclei are most efficient in increasing the spin lattice relaxation and will give the least value for T_1, which will further increase. So, in short, we can say that we will get spin-lattice relaxation minima when the rate of molecular motion is very close to RF value. On the other hand, T_2 values will keep decreasing even more as the molecular movements become slower, but T_1 values would start increasing. The relationships of T_1 and T_2 with v_0 and correlation time can be described using the following expression:

$$\frac{1}{T_1} = \gamma^2 \overline{H^2} (\frac{\tau_c}{1 + (2v_0\tau_c)^2})$$

$$\frac{1}{T_2} = \gamma^2 \overline{H^2}(\tau_c + \frac{\tau_c}{1 + (2v_0\tau_c)^2})$$

Here $\overline{H^2}$ symbolizes the mean square average of local magnetic field, which is a measure of the interaction strength between the spin of nuclei and the oscillating magnetic fields, with the correlation time of τ_c, which can be defined as a quantitative measure of the rate of molecular motion. In the case of translational movement, correlation time (τ_c) is the required average time for the tumbling of molecules through a distance equal to its diameter value. But, in case of rotational motion, it's necessarily the average length of time taken to rotate by an angle of around 33°. [8]

As implied by the above equation, these interactions with the minor random fluctuations in the magnetic fields cause spin-lattice relaxation in the most efficient way, due to the effect of molecular motions with correlation time:

$$\tau_c = 1/2\pi v_0$$

Such random local magnetic-fields are also responsible for spin-spin relaxation, but here these relaxation processes become more efficient as the motions become slower, which means τ_c is longer, as the local magnetic fields tend to be more static.

The line width of an NMR peak at half height, $W_{1/2}$ depends on T_2, which can be expressed by the following relationship:

$$W_{1/2} = 1/ (\pi T_2)$$

However, the point to keep in mind is that T_2 is not the only factor that contributes to line broadening; samples containing macro-molecules and some other factors could also contribute in making of the NMR signal broader than T_2 processes would, but it all depends on the surrounding of the molecule.

Consequently, from our understanding and above discussion, we will expect that an NMR peak of macro-molecules (or any ligands connected to that) will be relatively much broader as compare to signals of small molecules that are free to move in solution. This increase of broadening in the line is one of the major problems in performing NMR

studies of large macro-molecules like-proteins, because in the bigger molecules due to a higher number of different nuclei will increase the probability of signals from the various nuclei being overlapped/ crowded in an NMR spectrum. When these signals get broader, then resolution, as well as the amplitude of the different signals in the spectrum, will decrease. As a result, it could be even more challenging to do spectral analysis. Since the peak area under NMR signal is directly proportional to the amount of no. of nuclei present. The lowering in this amplitude intensifies the signal to noise problems of NMR, which can be understood in the context of the Boltzmann equation.

2.3 Diffusion NMR

Diffusion is defined as the random translational motion of particles/molecules that occurs due to their internal energy. This randomized translational motion leads to a collision between particles in a system, and as a result, chemical reactions take place. It can be described as one of the major factors, including activation energy and orientation of molecule, which causes almost all kinds of chemical reactions because the reaction species must collide to take place the reaction [18].

Translational diffusion is a very fundamental form of transportation in the biophysical and chemical systems. NMR spectroscopy provides a unique tool to measure it experimentally and quantify its behavior. [19, 20] Diffusion measurements in NMR are very suitable to understand the processes because of its noninvasive nature and potential to measure diffusion coefficient over a wide range of concentration and temperature. [21, 22] Diffusion can be understood in detail with Fick's laws of diffusion, given by Adolf E. Fick.

2.4 Fick’s laws of diffusion

To understand this, we can take a simple analogy. Let's say we have solute put inside a diffusing substance liquid as ink in water. Due to molecular collisions, this spreads throughout liquid uniformly. Hence, if there is some concentration of a molecular species solute inside a solvent, then it would typically spread out uniformly, just like ink in water.

This phenomenon can be understood by certain empirical laws known as Fick's laws of diffusion.

2.4.1 Fick's 1st law

Fick's 1st law explains how particles tend to spread out from a higher concentration region to a lower concentration region under random thermal motion. [23] It could be easily understood by a simple experiment when one opens a fragrance bottle at the other end of a closed room. After some time, the perfume odor spreads throughout the room because the perfume atoms tend to diffuse from a high concentration region to a low concentration region. [24] Mathematically, Fick's first law states that the diffusion flux is directly proportional to the concentration gradient ρ(r,t), which follows the continuity equation-

$$\dot{J} = -D\nabla\rho(\dot{r}, t)$$

For the 1dimentional system, above equation can be written as:

$$J_X = -D\frac{\partial\rho(x,t)}{\partial x}$$

2.4.2 Fick's 2nd law

Fick's second law explains how diffusion causes the change in concentration with respect to time. This change in the concentration of particles over time is equivalent to the change in local diffusion flux value, mathematically, it can be expressed as:

$$\frac{\partial\rho(r,t)}{\partial t} = D\nabla^2\rho(r,t)$$

$$\frac{\partial^2\rho(x,t)}{\partial t} = D\frac{\partial\rho(x,t)}{\partial x^2}$$

Where,

- ρ(r,t): The concentration gradient over space and time.

- r: the position vector.

- $\dot{J}$: The division flux of substance over per unit area and per unit time.
- D: A second rank diffusion tensor.
- t : Time in unit of second.

2.5 Stokes-Einstein equation

The Stokes-Einstein equation is used to calculate the diffusion coefficient of a "Stokes/spherical particle with a very small Reynolds number undergoing Brownian motion in a homogeneous material at a constant temperature.

$$D = K_B T/6\eta\pi r$$

Where

- D: Diffusion constant [$m^2 sec^{-1}$]
- k_B: Boltzmann constant [$1.38*10^{-23}$] [m^2 kg sec^{-2} K^{-1}]
- T: Temperature [K]
- r: Hydrodynamic radius [m]
- η: Dynamic viscosity of the medium [Pa-sec]

2.6 Pulsed Field Gradient Spin-Echo (PFG-SE) pulse sequence

In this technique, the attenuation of the spin-echo signal from the Hahn spin echo pulse sequence combined with a magnetic field gradient pulse in each time delay between the 90 and 180 pulse sequences applied to measure the displacement/ movement of observed spins. Therefore, in PFG-NMR, we consciously apply the gradient pulse for a small-time duration (δ), to bring spins along the z-direction and get additional component in frequency as:

$$\omega_{eff} = (\omega_0 + \Upsilon g_z Z)$$

The sole purpose of applying a homo-geneous gradient of known strength is to use larmor frequency as a spatial label by keeping to the direction of the gradient as reference, which further transformed into the cumulative phase shift. The degree of dephasing caused by gradient pulse is proportional to the strength of gradient pulse(g), duration of the pulse (δ), type of nucleus(γ), and the displacement of spins in the direction of the gradient.

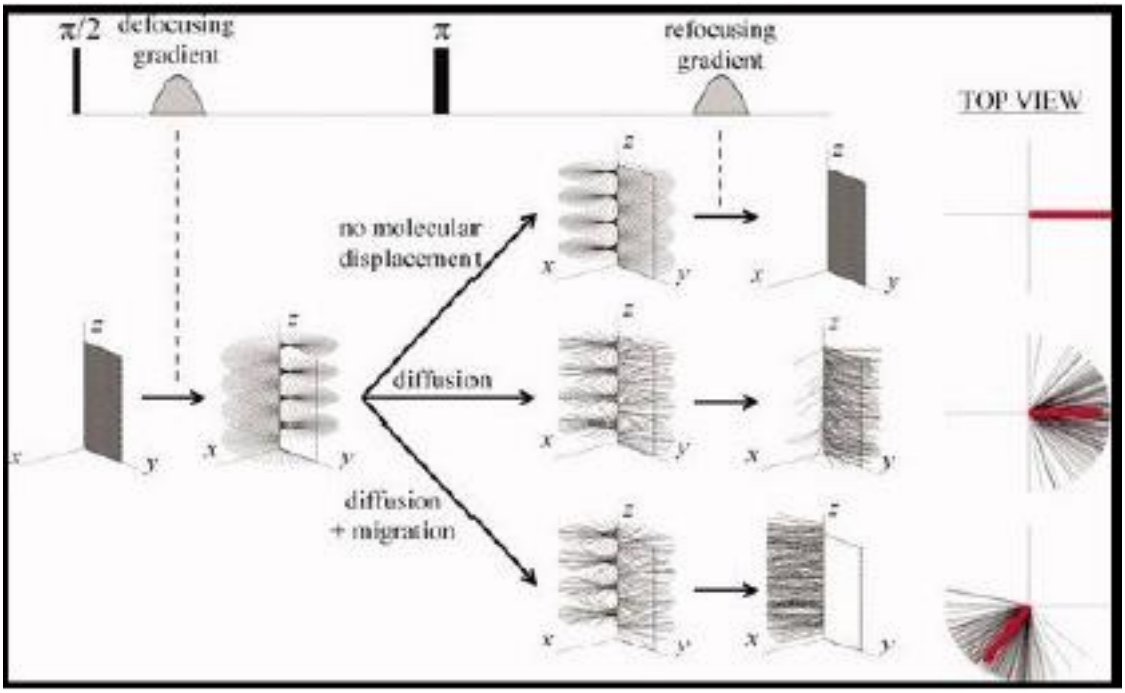

Figure 2.5 Pulsed Field Gradient Spin-Echo (PFG-SE) pulse sequence. [25]

In the figure 2.5, the PFG Spin echo pulse sequence and diffusion measuring phenomena are visualized by observing the NMR signal attenuation and its effect when there is no molecular movement, migration, and unidirectional translation [25].

2.6.1 Stejskal Tanner (ST) equation

The ST equation describes the signal attenuation at the end of the PFGSE experiment. This decay in signal is due to the loss of coherence during diffusion, which follows the following equation [26]

$$\frac{I}{I_o} = \exp[-(\gamma\delta g)^2 D(\Delta - \left(\frac{\delta}{3}\right)]$$

Where,

- I: The intensity of the diffusion NMR peak.
- γ: The gyromagnetic ratio of nucleus
- g: Applied gradient strength of pulse [Gauss cm^{-1}].
- Δ: Diffusion time [Sec.]
- D: Diffusion coefficient [m^2sec^{-1}]
- δ: Diffusion pulse gradient duration [Sec.]

Chapter 3

Ionic Liquid (BMIM Br) and Drug (5-Fluoro Uracil)

3.1 Introduction

Relaxation and diffusion NMR experiments have the potential to give valuable insights into the internal molecular dynamics and the overall hydrodynamic behaviour of folded and partially unfolded state. Fluctuations in the local dynamics can be correlated with a fondness for local compaction of the alkyl side chains, which can cause squeezing of motions. Such measurements can also provide insights into the effects of denaturants both on the overall hydrophobic behaviour of a drug in ionic liquid and upon its local structural arrangement. The dynamics can further be understood by measuring the T_1 and T_2 relaxation, diffusion coefficient, and the $\{^1H\} -^{19}F$ NOE experiments.

3.2 5-Fluoro Uracil (Antitumor Drug)

5-Fluorouracil is the backbone of modern chemotherapy which is extensively being used as an antitumor drug since 60 years, from the time it was first discovered by Heidelberg et al. [27] for the development of new strategies to effectively boost the antitumor activity of 5-Furacil, it has been extensively studied in photo physical and medical fields for the deeper understanding of its action mechanism. However, the drug resistance due to bacterial evolution will always remain a major concern for the clinical practice of 5-FUracil. Because of this drug resistance, 5-FUracil doses are given in higher quantity, this range varies micro-mill molar (mM) concentrations, and the use of high concentration may cause some side effects like- hepatotoxicity and cardio toxicity. [28, 29] When 5-FUuracil insert inside the cell of bacteria, it got converted into 5-fluorodeoxyuridine monophosphate (5-FdUMP). This 5-FdUMP competes with deoxyuridine for an enzyme thymidylate synthase (TS), which participates in the conversion of deoxyuridine monophosphate to deoxythymidine monophosphate (dTMP). But when 5-FUracil interact with TS, it interrupts the formation of dTMP which cause DNA synthesis to stop, as a result, bacterial cell dies. [30]

The 5-FUracil structure contains two strong hydrogen-bond donor (−NH) and one H-bond acceptor (−CO) groups. These groups guide the self-aggregation process of the drug. It was discovered that 5-FUracil forms ribbon like morphology by using two pairs of hydrogen-bonds between −CO, and –NH. The vital contribution of hydrogen bonding formation in case of aggregation of small molecules was reported in the literature. [31, 32].

N-methylation at the 1, 3- positions of 5-Furacil synthesize 5-F-1, 3-dimethyl uracil (5-FDMU), which lacks potent hydrogen-bond donors due to the replacement of proton by -CH3 group. In the case of 5-FDMU, stabilizing forces, dipole-induced dipole interactions, and hydrogen bond CH···O are weaker as compared to NH...O of 5-Furacil. It shows the effect of methylation on the self-aggregation of 5-Furacil and indicates that hydrogen bonding plays a prominent role in the self-assembly of small molecules. Many studies show that *N*-methylated derivatives of 5-Furacil (like--gemcitabine and capecitabine) are more effective than simply 5-FU, with fewer side effects in the cancer treatment. [33, 34]

The above-mentioned explanation makes it clear that self- assembling nature of drugs makes it less effective and increases the side effects and requires higher dose concentration for the treatment of cancer.

3.3 ^{1}H and ^{19}F NMR spectral assignment of 5-Furacil

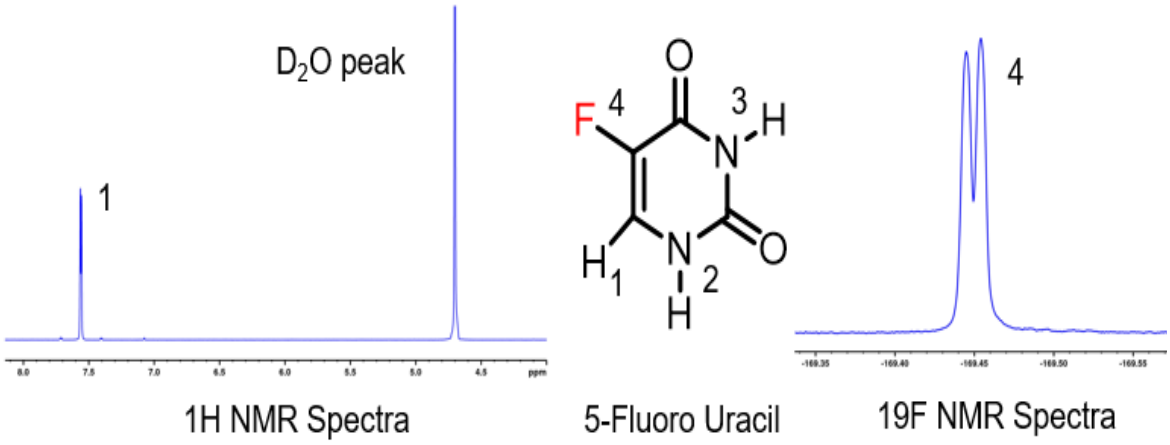

Figure 3.1: Molecular structure, ^{1}H and ^{19}F-NMR spectrum of an antitumor drug (5-Fluorouracil)

In the proton spectrum of 5-Furacil, there is only one doublet peak of (H1), this doublet is due to the $^{3}J_{H\text{-}F}$ coupling of (H1) with its neighboring (F4) nuclei. The rest two –N-H proton peaks did not appear in the ^{1}H NMR spectrum due to the very labile nature of N-H proton; it got to exchange with D_20 and end up resulting in a very broad peak.

In the ^{19}F spectrum, there is only one doublet peak of (F4) nuclei due to coupling with $^{3}J_{F\text{-}H}$ couping to its adjacent (H1) proton. Due to high senstivity and less noisy spectral qualities. ^{19}F-NMR studies will be our main intrest in this work.

3.4 Relaxation (T_1, T_2) and Diffusion data analysis of Drug in D_2O

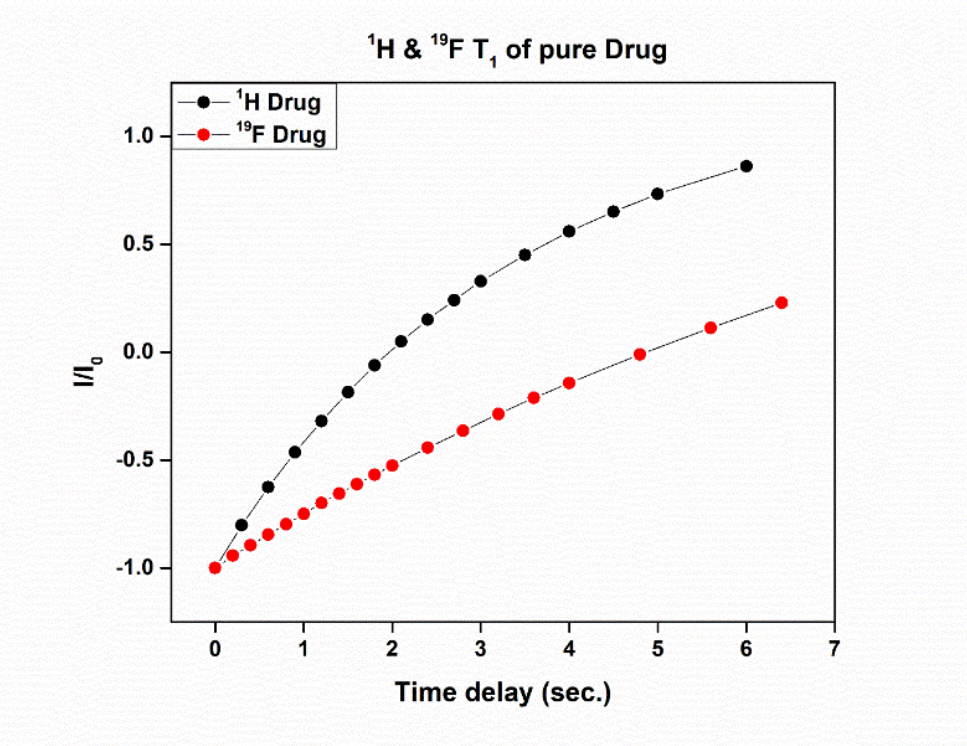

Figure 3.2: ^{1}H and ^{19}F longitudinal relaxation time (T_1) plot of pure drug at 298K

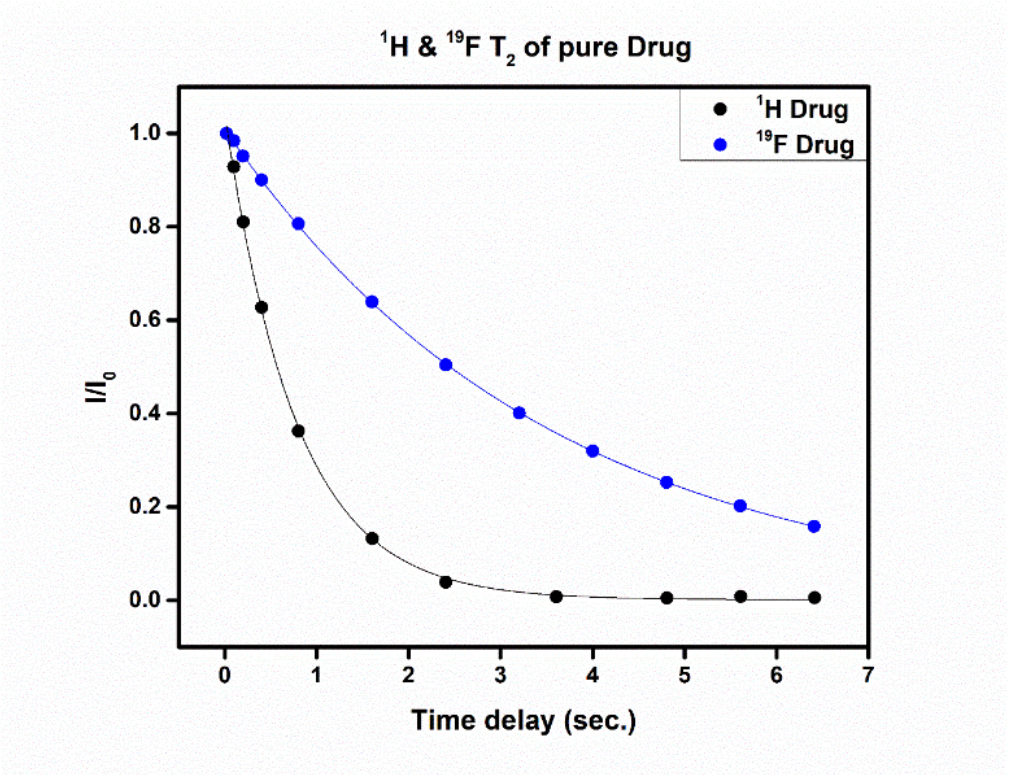

Figure 3.3: ^{1}H and ^{19}F transverse relaxation time (T_2) plot of pure drug at 298K

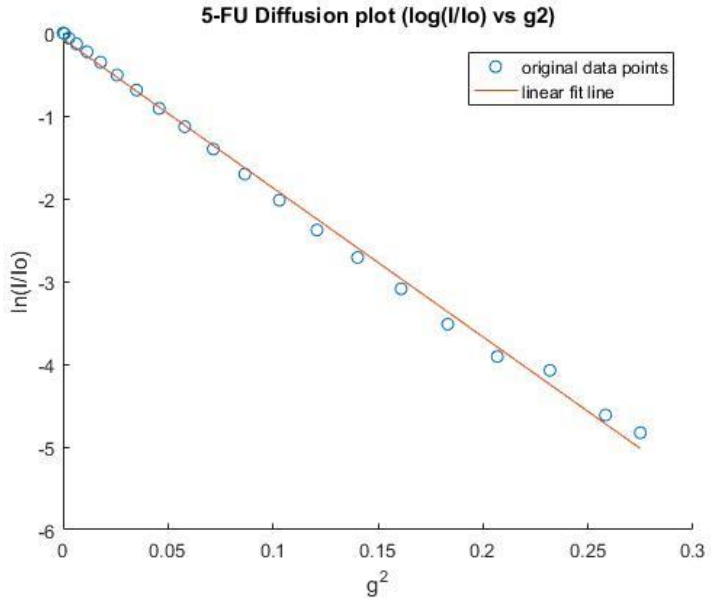

Figure 3.4: ^{1}H Diffusion plot of pure Drug at room temperature

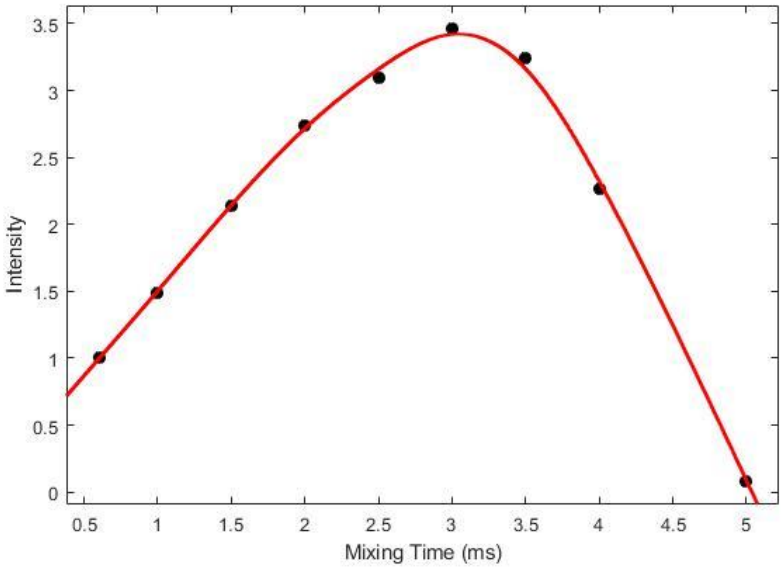

Figure 3.5: 1D ^{19}F- ^{1}H HOESY buildup curve of pure Drug at 298K

Sample	Nuclei	T_1(Sec.)	T_2(Sec.)	D*10^{-8} m^2/sec.	σ(sec.)$^{-1}$
30mM of 5-F-Uracil	^{19}F	2.22	0.98	2.49	0.48
	^{1}H	6.33	3.49	1.33	

Table 3.1: Relaxation time (T_1&T_2) and Diffusion coefficient values of 5-Furacil using ^{1}H and ^{19}F-NMR

30 mM Sample of 5-Furacil was prepared in D_20 and then spectral assignment of ^{1}H and ^{19}F NMR (see figure 3.1) were done to identify which signal belongs to which nuclei. After successful assignment of peaks, we focused on the peaks of our interest of Nuclei, which is (H1) and (F4) (as per figure 3.1).

Then longitudinal (T_1) and transverse (T_2) relaxation times were measured using t1ir1d and CPMG pulse sequences and data processing was done using topspin 3.7. Then plots of Intensity Vs time delay were plotted and data fitting was done as per exponential functions which define the recovery and loss of magnetization (explained in section 2.1 Relaxation). Similarly, diffusion experiments were performed using PFG-Spin echo pulse sequence by increasing the gradient power from 2-98 % in 21 steps and then data fitting was done in MATLAB.

These relaxation times, T_1 and T_2 values gives us information of the surrounding of nuclei and tells how fast or slow spin relaxing on the other hand diffusion coefficient tells us the movement of molecule in solvent medium, how fast and slow its moving in solution.

The ^{1}H-^{19}F 1D hoesy experiment gives us the information of cross relaxation rate of nuclei which can further be converted into distances and can give us the location of nuclei of interest in solution

3.5 What are Ionic liquids?

Ionic liquids are a class of molten salts at ambient temperature. Which have attracted considerable attention because of their unique properties such as non-volatility, non-flammability, thermal stability, and high ionic conductivity. The key to applications of ionic liquids is that most are liquids below 373 K. This liquidity is achieved by tailoring the cations and anions to destabilize the solid-phase crystalline structure. However, there are no fixed rules to synthesize an IL; in general, this can be accomplished within a reasonably wide range of ion structures by adjusting symmetry and ion-ion interactions. Tailor-made ionic liquid for specific properties and applications in green chemistry and drug delivery is of the broad area of research (just like tailoring shape and size of nanoparticles). Each ionic liquid will have different solubilities for chemicals. Due to the

large number (millions) of cations and complex anions, there are almost unlimited permutations and combinations for a researcher to use in compound design.

One of the attractive aspects of ILs based on the 1-alkyl-3methylimidazolium $[C_nMIM]^+$ cation is their inherent amphiphilic characteristic as a surfactants in various conditions. Many studies have carried out to investigate the aggregation behavior of ILs in solutions to explain some unusual characteristics in various applications. Investigation of the self-aggregation formation of [bmim] $[BF_4]$ and 1-decyl-3-methyl imidazolium bromide $[C_{10}mim]$ Br, a long alkyl chain imidazole ionic liquid, tends to form micelles in water. On the other hand, [bmim] Br, a short-chain bromide ionic liquid did not form micelles Dorbritz and Gaillon et al. also observed that ($[C_{10}mim]$ Br) forms aggregates in the water at low concentrations and then self-assembles to form lyotropic mesophases at higher concentrations. [35, 36] These studies shows that length of attached alkyl chain is a deciding factor in micelle formation of IL, as in our target IL alkyl chain length is relatively small so it will not go into aggregation under normal conditions.

The aggregation formation study for [BMIM] $[BF_4]$ in ethanol, propanol, water, and ethyl acetate by using electrospray ionization mass-spectrometry techniques and conductivity analysis unveils that with a decreasing concentration of the IL and increasing polarity of the solvent, the size of the aggregate formation decreases.[37] On the basis of turbidity and conductivity measurements, phase structural studies, surface behavior and aggregation of $[C_nmim]$ Br-water mixtures can be explained using a variety of methods. Considering the fact that nuclear magnetic resonance (NMR) is a very sensitive technique for the study of the aggregation behavior and possible microscopic structures of classical surfactant, [BMIM] Br ILs in D_2O by using ^{1}H-NMR and 2-Dimentional ^{1}H-^{1}H NOESY experiments. [38]

3.6 ILs in Drug delivery

Transdermal drug delivery advances an easy mode of regulating drugs while simultaneously maintaining a strategic distance avoiding the tricky first pass metabolism. However, passing through the uppermost transport hindrance of skin-layers, the stratum corneum (SC), is a crucial step. The SC comprises of a firmly packed brick and mortar-like structure of corneocytes, compressed by the lipids. [39, 40]

Fewer drugs possess lower mass, and higher lipophilicity are equipped for exploring the SC boundary without assistance. A few techniques have already been engineered to improve skin permeability for drugs, including the utilization of ultrasound, iontophoresis, micro needles, pervasion enhancers, and stream injectors, etc. Currently, ionic liquids and profound eutectic solvents, sometimes collectively addressed as ionic liquids and have shown some extraordinary work for drug delivery. An aggregate label alludes to these two different types of materials to concentrate on their properties instead of definitions. ILs have indicated an incredible outlook for transdermal drug delivery, including the delivery of proteins and various small molecules. [41, 42]

The adequacy of ILs in upgrading skin permeability is relied upon on their creation and ionic constituents. However, the summed-up comprehension of the role of ion properties in deciding IL's delivery potential is still inadequate. Numerous different sorts of transdermal delivery advances have profited by nitty- gritty investigations of their parameter sensitivities and key mechanisms. Specifically, in the case of chemical permeation enhancers, enhancement dependence on the enhancers' chemical structure and Computational studies have confirmed molecular mechanisms of enhancers. [43, 44] Such investigations with the chemical enhancers have prompted engaging experiences into their action mechanism as well as the design and synthesis of novel penetration enhancers. However, such detailed literature for ILs are still lacking.

3.7 Proton NMR spectral assignment of [BMIM] [Br], IL

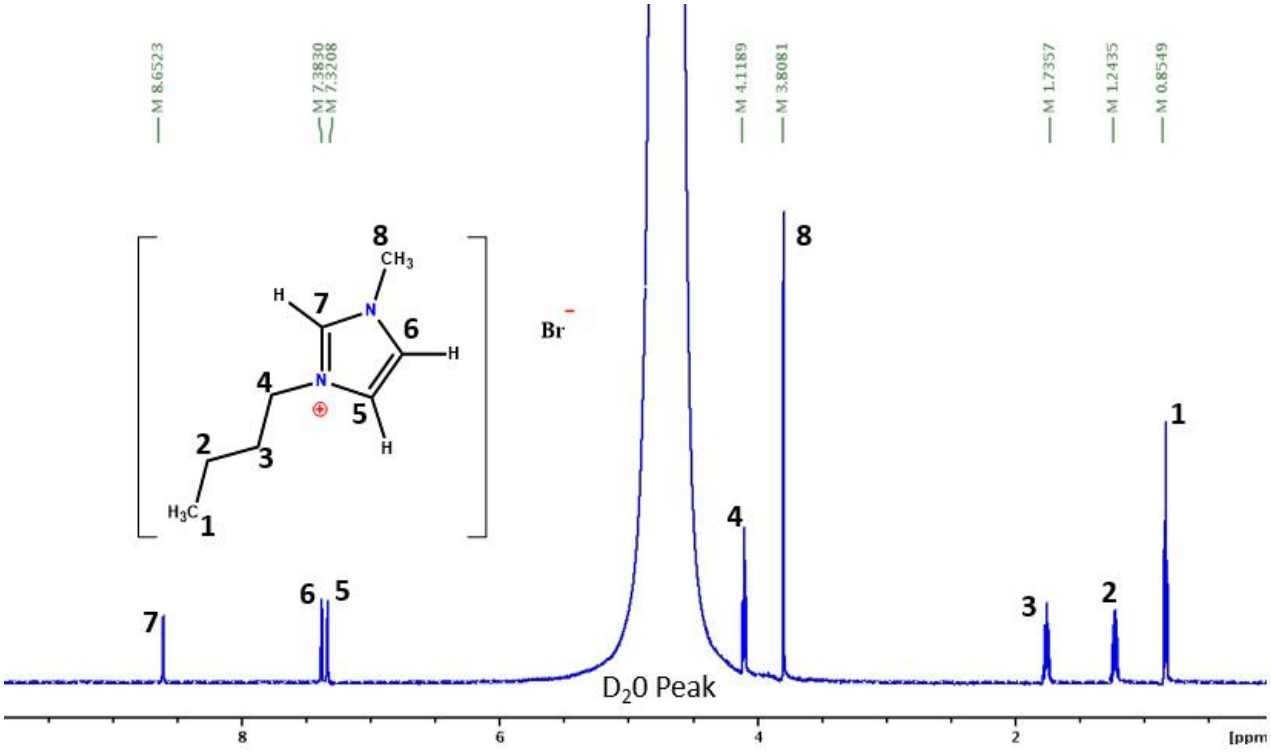

Figure 3.6 ^{1}H NMR spectrum and structure of (4-Butyl-3-Methyl imidazolium Bromide)

The spectra of ionic liquid (1-Butyl-3-Methyl imidazolium Bromide) shows eight different peaks in ^{1}H NMR. This clarifies that the ionic liquid exhibits eight different types of protons.

All protons show different chemical shift values according to their chemical environment. Proton assigned number 1 in the structure, which is on the primary carbon atom, shows peak value at 0.85 ppm with triplet splitting, following (n+1) splitting rule. Number 2 proton shows multiplet at 1.24 ppm similarly number 3 proton shows multiplet. Proton present on number 4 felt downfield due to the N-atom present next to it and shows a peak at a higher value. Proton on number 5 and 6 are aromatic protons and shows doublet at 7.32 ppm and 7.35 ppm. Number 7 proton faces maximum deshielding due to the two N-atoms that leads to the peak value at 8.65ppm. The other proton on number 8 shows singlet at 3.80ppm, which is slightly deshielded as compared to proton 1 due to the presence of electron-withdrawing N-atom next to it.

3.8 Relaxation (T_1, T_2) and Diffusion data analysis of [BMIM] [Br], IL in D_2O

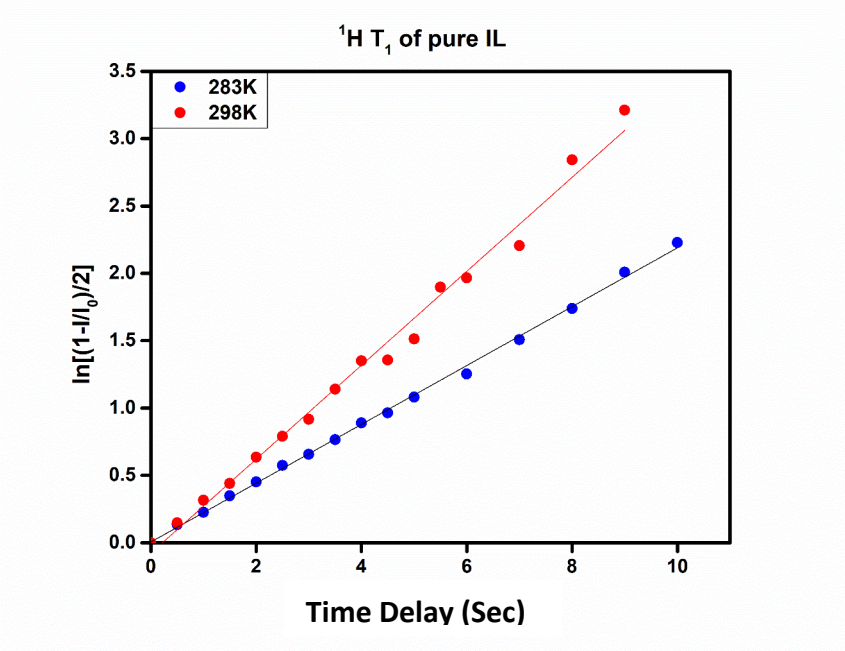

Figure 3.7: Intensity Vs time delay plot of ^{1}H longitudinal relaxation time (T_1) of pure IL at 298 and 283K.

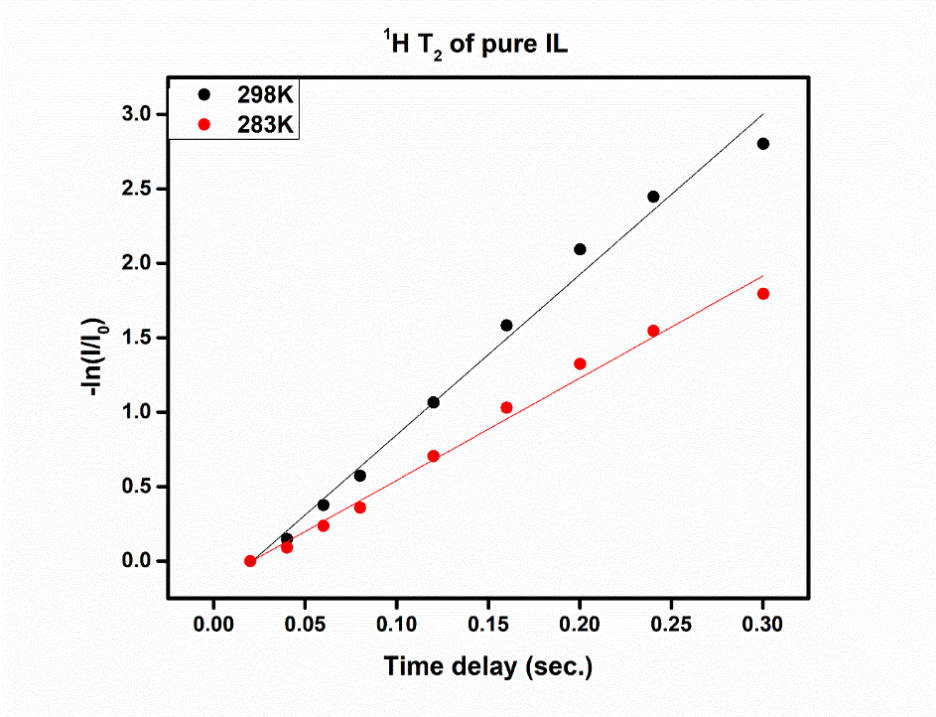

Figure 3.8: Intensity Vs time delay plot of ^{1}H transverse relaxation time (T_2) of pure IL.

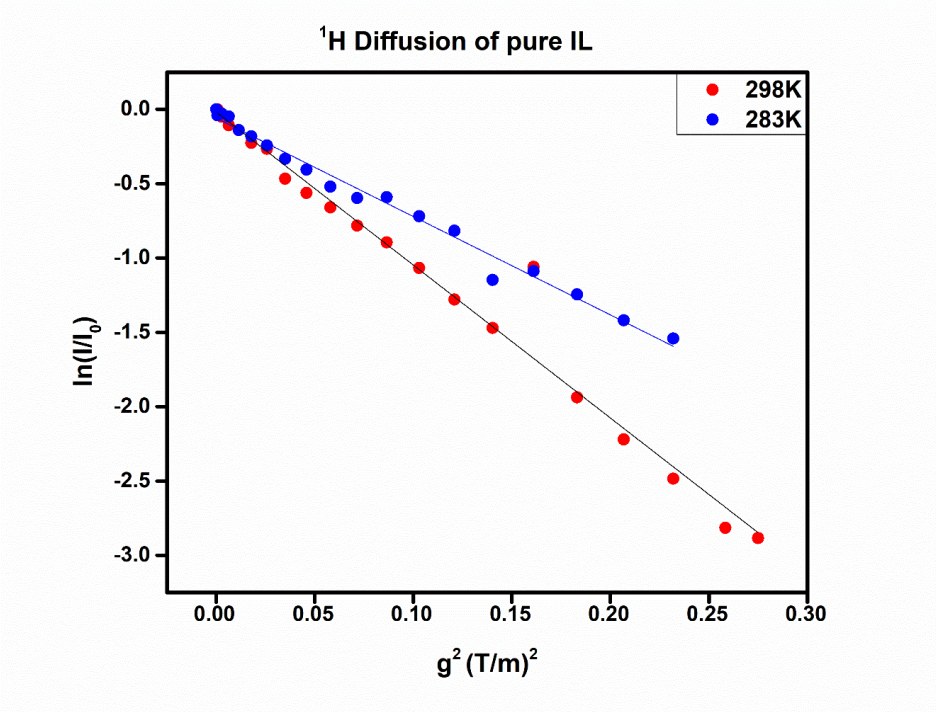

Figure 3.9: Intensity Vs g^2 plot of ^{1}H Diffusion for pure IL at 298 and 283K.

Sample	Nuclei	Temperature	T_1(Sec.)	T_2(Sec.)	D*10^{-8} m^2/sec.
150mM of $[C_4MIM]^+$ $[Br]^-$	^{1}H	298 K	4.512	0.183	0.716
		283 K	2.568	0.169	0.484

Table 3.2: Relaxation time (T_1&T_2) and Diffusion coefficient values of BMIM Br using ^{1}H-NMR at different temperatures.

BMIM Br, IL sample were dissolved in D_2O and proton spectral assignment was done (Figure 3.8). ILs are temperature sensitive so T_1 and T_2 experiments were performed at two different temperatures and shows distinct values at each case, at higher temperature kinetic energy of molecules increases and as result tumbling and movements of molecule

increases, these are the information that we got through relaxation times that's why here T_1 and T_2 increases with temperature.

Diffusion coefficient of IL is also increasing with the increase of temperature and follows Arrhenius relation-

$$D = D_0\, e^{-E_a/RT}$$

Chapter 4

Methodology, Results and Discussion

4.1 Introduction

In this work, I have used ^{19}F and ^{1}H NMR spectroscopic techniques to study the solvation mechanism and dynamics of 5-Furacil in [BMIM][Br], focusing on the ions of the Ionic liquid and the 5-Furacil molecule. This study depends on the monitoring of the hydrogen-bonding behavior between drug-IL molecules, which seems to be a major factor for the dissolution of the drug over the wide range of IL concentration. In addition to that, I have done some density functional theory (DFT) calculations to validate the experiments and for the prior understanding of the system. Moreover, 2D ^{1}H- ^{1}H NOESY and ^{1}H-^{19}F HOESY NMR experiments were done to probe proximity between IL ions and drug molecule. These experiments should be able to propose a primary interaction model to understand the dissolution of 5-Furacil in the IL 1-Butyl-3-methyl imidazolium bromide.

4.2 Computationally optimized Drug-Ionic liquids interaction model

4.2.1 Gaussian Calculations

Gaussian is an electronic computational chemistry software package capable of predicting several properties of molecules, atoms, and reactive systems using ab initio, density functional theory (DFT), and other basic quantum mechanics laws. To predict properties of reactions and molecules, including bond and interaction energies, molecular energies and structures, NMR shielding and magnetic susceptibilities.

We are doing quantum calculations using Gaussian 09 to get the most stable structure, energy of the structure, and possible interaction sites of molecules under a wide range of possibilities, including both stable species and compounds which are difficult to observe experimentally or to know the most energetically stable interaction site before starting our experiments.

4.2.2 Levels of Theory

The level of theory is the collection/set of some underlying approximations applied to define the chemical system. A higher level of theory provides more accuracy, however, at a greater computational cost.

1 Semi-empirical - (PM3, AM1, MNDO …)

2 Ab initio: (Hartree Fock, MP2, CCSD (T) …)

3 Density functional theory: (DFT) - (B3LYP…)

4.2.3 Ab initio Method

The important thing about this method is that it is wholly based on theoretical principles without the use of experimental data. There are a large number of methods that have the same basic approach, but they all are different in the use of mathematical approximations. These methods got much more popularity despite having a long calculation time.

Example of Ab initio Methods-

Hartree-Fock:

Hartree Fock is an elementary version of ab initio model. It is mostly based upon the approximation in which averaged coulombic electron-electron repulsion is considered instead of explicit repulsion interactions, also known as central-field approximation. In this, there are two separate methods to compute molecular orbitals:

- Restricted Hartree Fock
- Unrestricted Hartree Fock

Restricted Hartree Fock utilizes the spatial function of same orbital for every electron within the same pair, used for paired species, and without any spin contamination. Unrestricted Hartree Fock uses a separate orbital for every single electron, even if electrons are paired. It's suitable for excited states, radicals, ions, etc.

4.2.4 Density Functional Theory

Density functional theory methods are gaining more popularity because it provides an alternative approach to electron correlation. The results found by this method can be compared with the results obtained from ab initio methods with the drastically reduce CPU time. This method aims to determine functional connecting electron density with energy. This method is quite different from the ones which are based upon Hartree Fock calculations. So, In the case of DFT, the electron density is utilise to compute the energy, whereas for HF wave function is used.

Ex. of DFT Method-

B3LYP - It is the most popular DFT method, which uses corrections of both exchange energy and gradients that's it's known as a hybrid.

4.2.5 Basis Set

It is a set of wave functions which is used to elucidate the shape of atomic orbitals. For the computation of molecular orbitals (MOs), there are some predefined theoretical models by linearly combining the Atomic orbitals. The basis set is not required for work by all the theoretical models. Just as an example: PM_n (n=3, 4....6) models make use of their internal basis set. Others like ab initio or DFT needs specific basis set to function.

The approximation level of calculations depends upon the use of the basis set.

For example: - 3-21G, 6-311G(d,p).

Where 6-311G represents-

6 GTOs for core orbitals, 3 GTOs for inner valence, 2 different GTOs for triple zeta.

4.2.6 Proposed Interaction Model

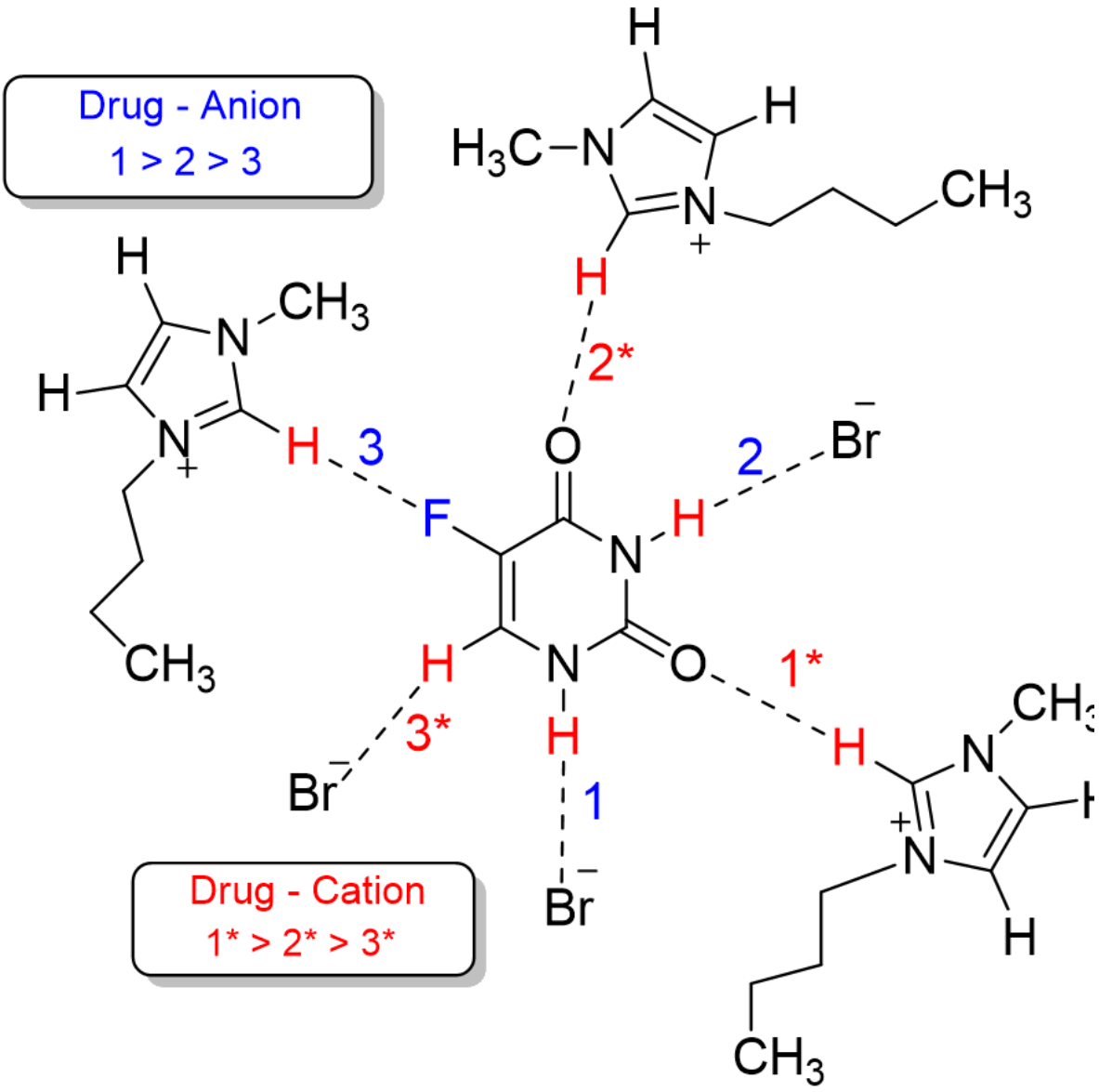

Figure 4.1: Gaussian optimized Drug-IL interaction model

From previous study, we knew that 5-Furacil is more effective for treatment of Skin cancer when we dissolve it in BMIM Br as compared to water. Also, in IL its solubility increases 2.5 times as compared to water. So, in order to understand the dynamics of 5-

furacil in BMIM Br, I have done some Gaussian calculations and proposed a 5-Furacil-BMIM Br interaction model.

To compute this model, I optimized the individual structure of 5-Furacil and BMIM Br at lower level of theory (HF), the use of Restricted and Unrestricted Hartree Fock method depends on the type of molecule (Detail in section 4.23), and the used basis set was 6-311. After successful optimization of Drug and IL molecule, I used these optimsed structures to calculate the interaction energy of Drug-IL at DFT – B3LYP level of theory and 6-311 G(d,p) basis set, a higher level of theory which has higher computation cost.

As IL has 8 different kind of proton but most labile proton (Proton in red) will interact with electronegative atom and form weak hydrogen bond. So, oxygen of carbonyl (–C=O) group and F nuclei is possible interaction site for cationic part of IL and Br^- of IL can interact either at 2 (-NH) group or –CH proton. So I performed energy calculation for 6 different scenarios (3 for cation and 3 for anion of IL). Most stable interaction geometry should have least energy of stabilization, so, I have arranged the stability order of structure or preferred interaction side on the basis of these energy values.

This order is as follows:-

- Drug-Cation → $1^* > 2^* > 3^*$
- Drug-Anion → $1 > 2 > 3$

For notation and other details look at figure 4.1

After getting insight of possible interaction site of Drug-IL, we further designed our NMR experiments to confirm the computational results.

4.3 NMR Sample Preparation

1. As 5-Fluorouracil is soluble in water, so 60mM concentration stock solution of 5-Furacil was prepared in D_20 and centrifuged to get a homogeneous solution.
2. ILs are hygroscopic in nature; they can easily capture moisture from the surrounding environment. So, to avoid that problem, we done the sample weighing part in glove box at 0.049 mbar pressure and 60 °C temperature.
3. Then, 300 mM concentration stock solution of BMIMBr (ILs), was prepared in D_20.
4. To study the effect of IL's concentration on drug dynamics, five samples of Drug-IL mixtures were prepared with the increasing concentration of IL while keeping the drug concentration constant.
5. Detail stoichiometry of Drug-IL mixture's sample preparation can be followed as given in the table below:

Drug Volume (µL)	IL Volume (µL)	Drug : IL Composition (mM : mM)	Concentration Ratio
250	50	30:30	1:1
250	100	30:60	1:2
250	150	30:90	1:3
250	200	30:120	1:4
250	250	30:150	1:5

Table 4.1: Stoichiometry of Drug and IL used in NMR sample preparation

6. In order to record NMR spectra, each sample mixture was poured into a 5 mm NMR tube, and then the total volume of the sample was makeup to 500 uL using D_2O.
7. The samples were kept overnight to give sufficient time for Drug-IL binding, and then NMR experiments were performed as per requirements.

4.4 Used NMR parameters

The NMR experiments were performed on the Bruker Avance-III 600 MHz NMR spectrometer equipped with a 5 mm QXI probe. The standard Bruker pulse program zg30, zgflqn, t1ir1D, CPMG, and PFG-SE were used to record 1D proton, ^{19}F, T_1 relaxation, T_2 relaxation, and diffusion spectra, respectively. Diffusion experiments were done with a single axis actively shielded z-gradient, with the capacity of achieving a maximum gradient strength of 53.5 Gcm^{-1}. Relaxation experiments (T_1 & T_2) were performed for different relaxation delays.

Some experiments were performed at ambient temperature (in an air-conditioned room at 22^0 C), while a few experiments were performed at a constant temperature using the temperature probe for the Drug-IL mixture. NMR data processing was done using Bruker Topspin 3.7 and Mnova software. One dimensional ^1H and ^{19}F spectra were recorded for the Drug and IL samples with 20 ppm proton spectral width using experimental parameters: number of scan = 16, processed with SI = 64k, TD = 132k, D1 = 1s and line broadening (LB) = 0.3Hz.

^1H and ^{19}F Relaxation experiments were done using t1Ir and CPMG pulse sequence by varying relaxation delay 0.0-8.0sec. Similarly, ^1H and ^{19}F diffusion experiment Pulse sequence 'ledbpgp2s1d' was used for diffusion experiment with maximum gradient 53.5 G/cm.

Experimental parameter: 16 scans, 1-2 ms gradient pulse (δ = P30 × 2), gradient recovery delay 200μs, and a diffusion delay (Δ) = 100-500 ms were used for the different molecules. Experiments were done for different gradient intensity varying from 2-98%, and then processing was done using Topspin 3.7 software.

4.5 Drug-IL NMR spectra at different temperatures

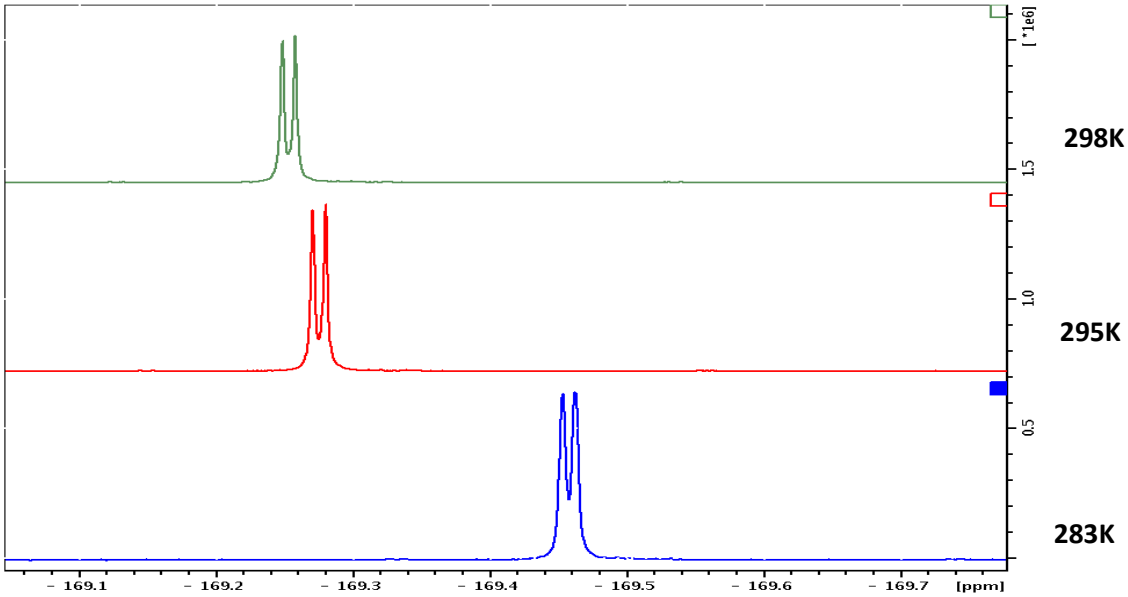

Figure 4.2: ^{19}F -NMR spectras of 1:3 Drug-IL mixture at three different temperatures.

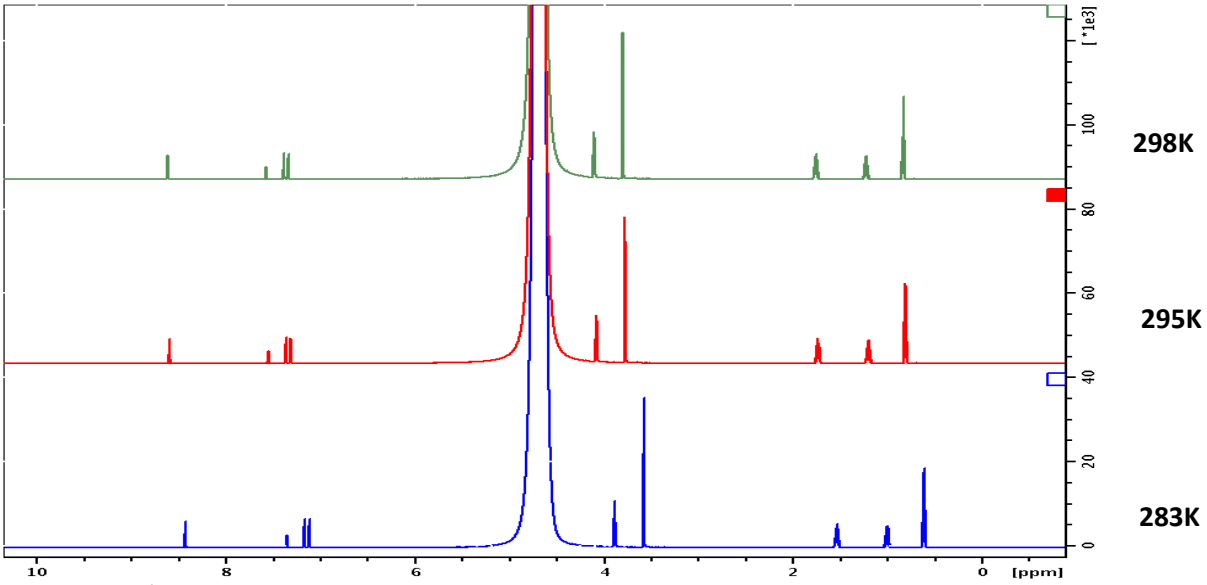

Figure 4.3: ^{1}H -NMR spectras of 1:3 Drug-IL mixture at three different temperatures.

The figure 4.4 and 4.5 contained a series of ^{19}F and ^{1}H NMR spectra of 1:3 Drug-IL mixtures with increasing temperature in upward direction. As can be seen, increase in temperature causes downfield shift in NMR spectrum for both nuclei.

4.6 Drug-IL NMR spectra for Different Concentration of IL

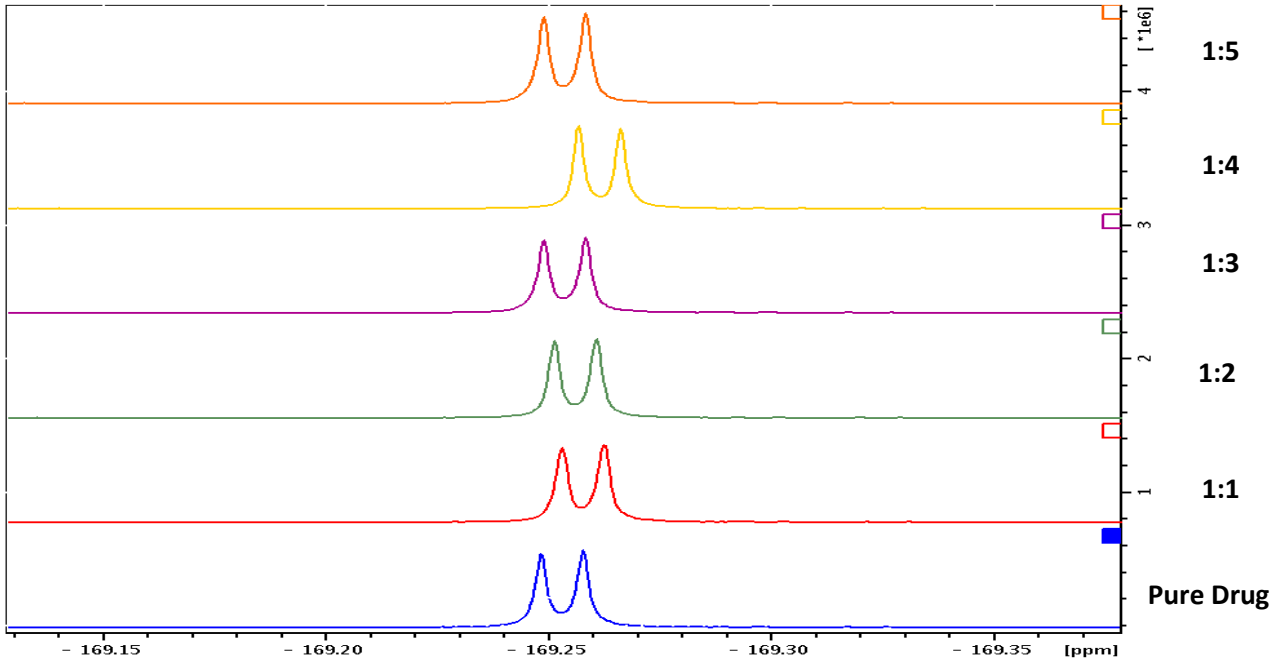

Figure 4.4: A series of ^{19} F-NMR spectrums of Drug-IL mixtures with increasing concentration of IL, starting from pure IL (Reference spectrum) to 1:5 drug-IL mixture.

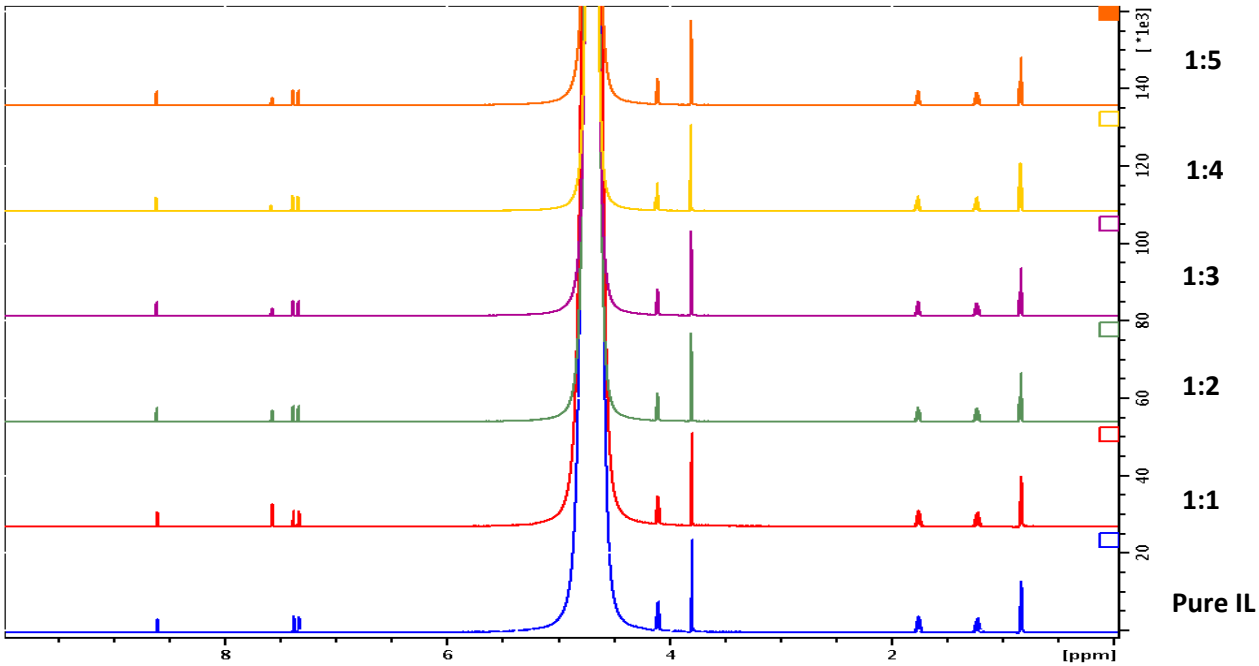

Figure 4.5: A series of ^{1}H-NMR spectrums of Drug-IL mixtures with increasing concentration of IL, starting from pure IL (Reference spectrum) to 1:5 drug-IL mixture.

Figures 4.4 and 4.5 contained a series of ^{1}H and ^{19}F NMR spectra of Drug-IL mixtures with increasing IL concentration. If we have a close look on both the spectrum (figure 4.4 and 4.5), we can see the up-field shift in ^{19}F peak among all spectra and very slight down-field shift in ^{1}H-NMR peak in (H7) of IL that suggest the change in the environment around nuclei of interest. From the above discussion, we know that there is a possibility of hydrogen bond between fluorine of drug and proton of IL (F…H), and hydrogen bonding decreases electron density around proton nuclei due to attachment of highly electronegative atom, which causes deshielding at proton nuclei and shielding at electronegative nuclei. That's why there is an up-field shift in fluorine peak and slight downfield for IL's (H7). But for IL, this downfield shift can be observed only between pure IL and Drug-IL mixture not among different mixture samples because in all mixture samples, the drug concentration is constant, but on the other hand, for fluorine nuclei, IL concentration is increasing.

4.7 Relaxation and Diffusion data analysis of Drug-IL mixtures at different Temperatures

4.7.1 For ^{19}F Nuclei

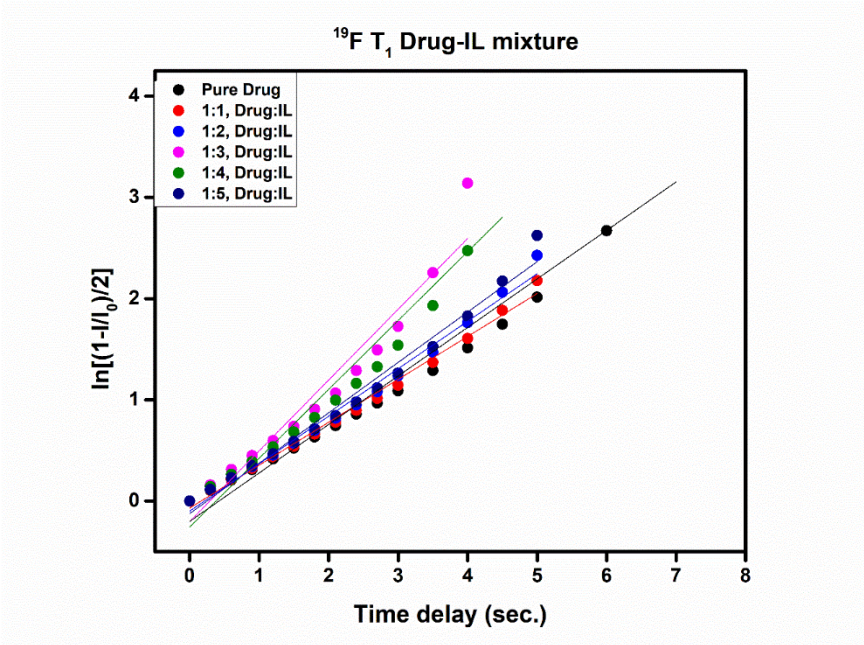

Figure 4.6: ^{19}F-Longitudinal relaxation time (T_1) plot of Drug-IL mixtures with increasing concentration ratio of IL at 298K

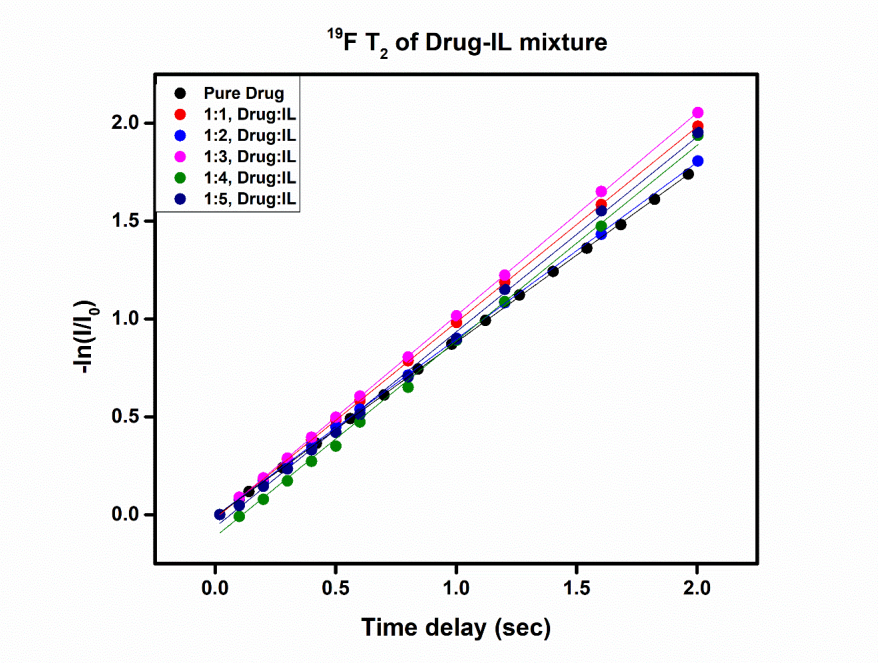

Figure 4.7: ^{19}F-Transverse relaxation time (T_2) plot of Drug-IL mixtures with increasing concentration ratio of IL at 298K

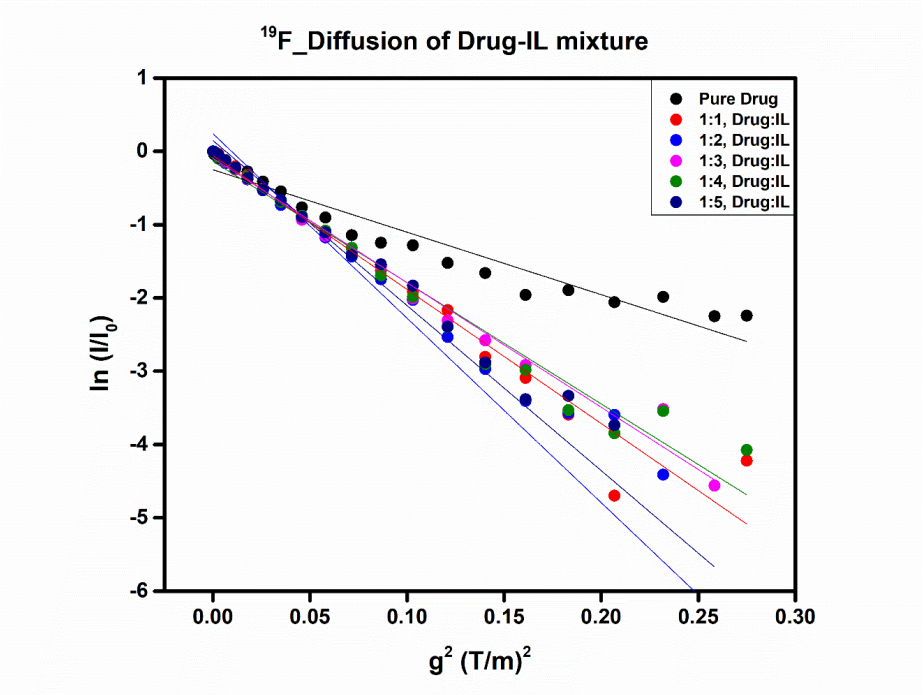

Figure 4.8: ^{19}F-Diffusion plot of Drug-IL mixtures with increasing concentration ratio of IL at 298K

Sample	^{19}F T_1 Relaxation			^{19}F T_2 Relaxation		
(Drug: IL) Mixture	Without temp. probe	298 K	283 K	Without temp. probe	298 K	283 K
Pure Drug	2.151	2.266	Poor data	0.985	1.133	Poor data
1:1	1.414	2.477	1.402	0.965	1.016	0.828
1:2	1.696	2.269	1.551	1.106	1.114	0.759
1:3	1.679	1.564	1.481	1.03	0.981	0.828
1:4	1.67	1.625	1.456	1.013	1.094	0.7
1:5	1.622	2.157	1.389	1.116	1.056	0.747

Table 4.2: Relaxation times (T_1&T_2) of 5-Furacil's F nuclei with increasing concentration of IL at three different temperatures using ^{19}F -NMR

Sample	^{19}F Diffusion ($D*10^{-8}$ $m^2/sec.$)		
(Drug: IL) mixture	Without temp. probe	298 K	283 K
Pure Drug	3.549	3.734	Poor data
1:1	3.139	3.506	2.548
1:2	3.040	3.238	1.980
1:3	2.742	3.289	2.543
1:4	2.708	1.990	1.990
1:5	3.370	3.308	1.914

Table 4.3: Diffusion coefficient values of 5-Furacil's F nuclei with increasing concentration of IL at three different temperatures using ^{19}F –NMR

Fluorine has the potential to plays a vital role in estimating the binding affinity and potency of the drug, along with fine spectral resolution and good NMR sensitivity and less crowded Heteronuclear experiment like 1D ^{1}H-^{19}F HOESY and other sets of NMR experiments can give us valuable insight of drug Dynamics. As per the above discussion (sec 4.2.6), we know that F nuclei of the drug is one of the possible interaction sites at

which (aromatic -CH) proton of IL's cation can interact and form a hydrogen bond (F…H).

In this work, ^{19}F relaxation and diffusion experiments were done for pure drug and then Drug-IL mixture with the increasing concentration ratio of IL at three different temperatures to observe the effect of IL environment on drug dynamics. Our Gaussian optimized interaction model gave us some pre-insight about the available number of interaction sites. According to which, more favourable and energetically stable sites are two carbonyls (-C=O) groups. Hence, when we use drug-IL in 1:1 and 1:2 ratio, it is highly probable that the cation of IL will interact at the carbonyl group. Still, once we further increase IL's concentration, there should be a weaker hydrogen bond formation between (F…H). The reason behind temperature depends on experiments- we all are aware of the fact that ILs are sensitive to temperature, and there can be structural changes and aggregation formation of ILs in specific temperature ranges. So, we decided to do relaxation and diffusion studies at different temperatures to observe its effect and change in dynamics.

The ^{19}F-NMR relaxation (T_1, T_2) and diffusion data is summarized in (table 4.2, and 4.3). As we can see the values of T_1 and T_2 (Table 4.2) for pure drug is higher but when we see the value for Drug-IL mixture it getting lower which is an indication of binding and change in dynamics. However, these values are expected to follow the decreasing trend with an increase in concentration, which is not the case for some samples.

A similar trend is expected with diffusion data because, with the increase of concentration of IL, the higher no. of IL molecules will be readily available and will have higher chances of interaction at multiple sites which will increase the overall size of the molecular cluster and will result in slower diffusion.

4.7.2 For ^{1}H Nuclei

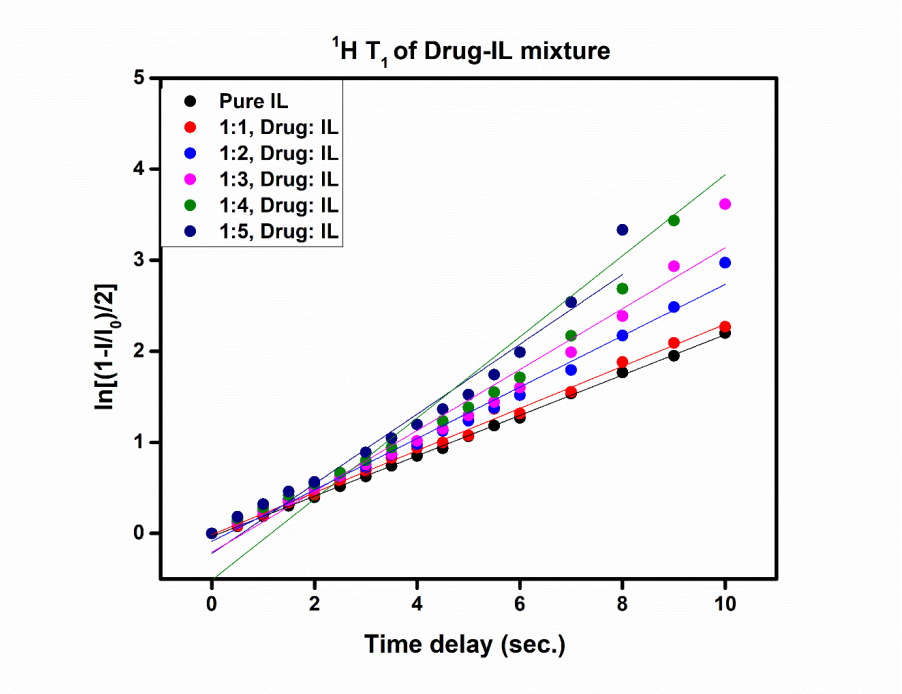

Figure 4.9: ^{1}H-Longitudinal relaxation time (T_1) plot of Drug-IL mixtures with increasing concentration ratio of IL at 298K

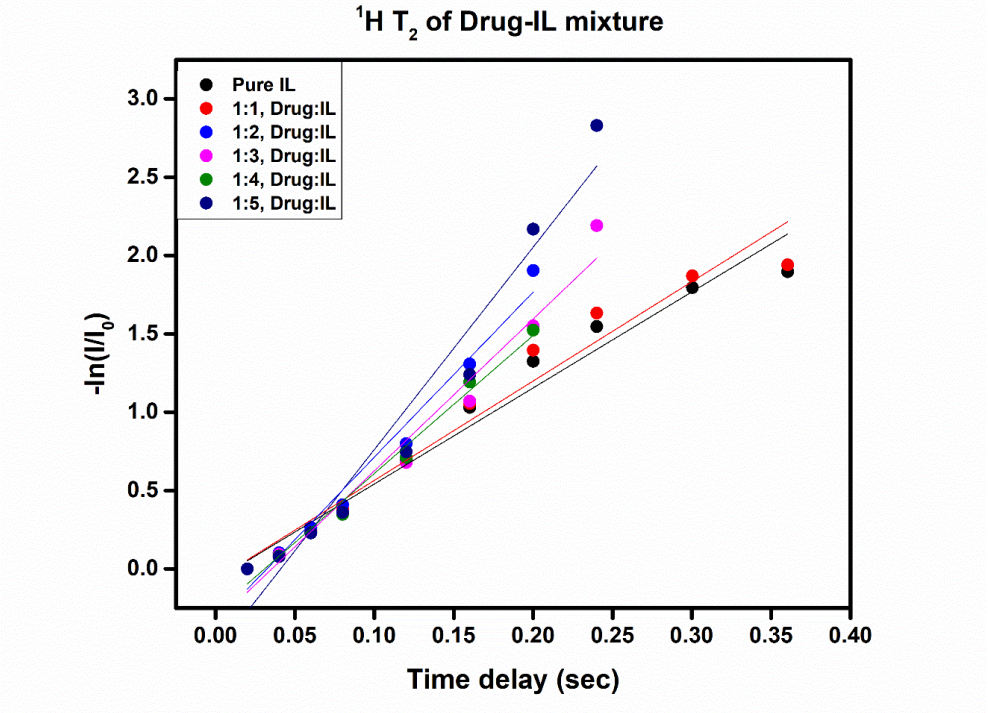

Figure 4.10: ^{1}H-Transverse relaxation time (T_2) plot of Drug-IL mixtures with increasing concentration ratio of IL at 298K

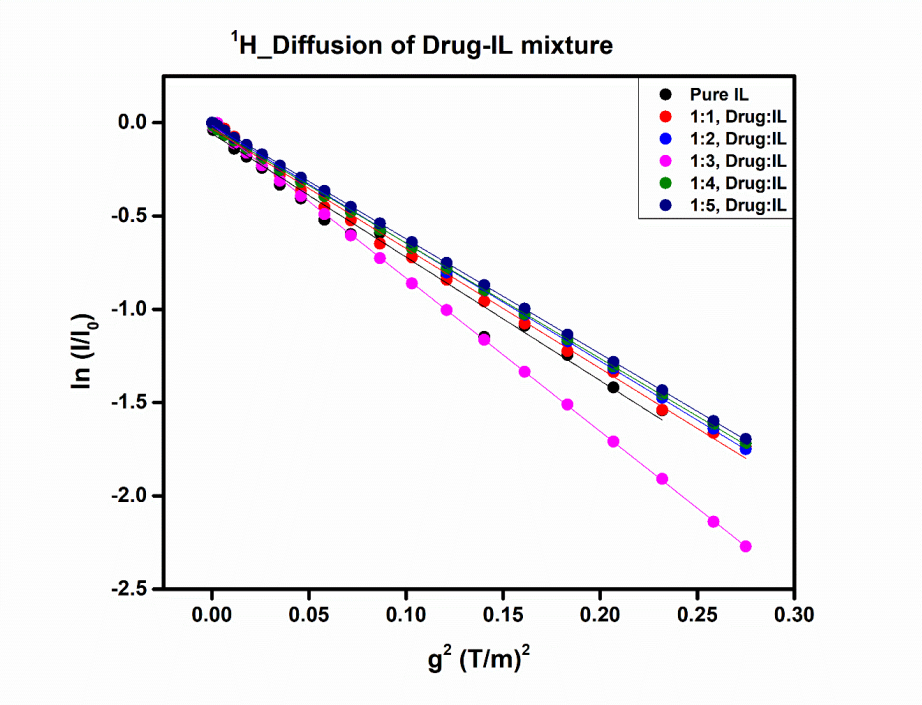

Figure 4.11: ^{1}H-Diffusion plot of Drug-IL mixtures with increasing concentration ratio of IL at 298K

Sample	^{1}H T_1 Relaxation (Second)		
(Drug: IL) mixture	Without temp. probe	298 K	283 K
Pure IL	4.622	4.512	2.568
1:1	4.363	3.882	2.471
1:2	3.709	4.297	2.756
1:3	3.261	3.894	3.963
1:4	3.098	3.103	2.611
1:5	2.857	3.297	2.471

Table 4.4: Longitudinal Relaxation time (T_1) values of 8.65 ppm signal of IL with increasing concentration of IL at three different temperatures using ^{1}H –NMR

Sample	^1H T_2 Relaxation (Second)		^1H Diffusion ($D*10^{-8}$ $m^2/sec.$)	
(Drug: IL) mixture	298 K	283 K	298K	283 K
Pure IL	0.183	0.169	0.716	0.484
1:1	0.154	0.163	0.726	0.455
1:2	0.159	0.119	0.722	0.441
1:3	0.179	0.126	1.072	0.571
1:4	0.615	0.141	0.725	0.436
1:5	0.707	0.097	0.707	0.427

Table 4.5: Transverse Relaxation time (T_2) and Diffusion values of 8.65 ppm signal of IL with increasing concentration of IL at two different temperatures using ^1H –NMR

As discussed in section 4.7, fluorine of drug interacts with most acidic/labile and aromatic proton (H7) of IL's cation. So, in order to confirm the point that whether this proton is actually forming a hydrogen bond or not, we have done relaxation and diffusion analysis of (H7) proton, which shows the peak at 8.65 ppm.

Relaxation times (T_1 and T_2) were measured using t1ir1d and CPMG pulse sequences, and data processing were done using topspin 3.7. Then Intensity Vs. Time delay graphs were plotted, and data fitting was done using defined exponential functions. In figures 4.9 and 4.10, T_1 and T_2 data are fitted for different drug-IL mixture with increasing concentration ratio at a fixed temperature. The slopes of these plots for different sample gives an indication of its relaxation values. Relaxation time is decreasing with the increase of IL concentration. T_2 value is a measurement of rotational and tumbling of molecules; lowering in relaxation times means a lack of free motion of molecules, which is most likely happening due to the binding of molecules.

Similarly, diffusion experiments for various Drug-IL mixtures were performed using the PFG-Spin echo pulse sequence by increasing the gradient power from 2-98 % in 21 steps, and then data fitting was done in MATLAB. Here, the slope of the graph represents the diffusion coefficient, so the plots in figure (4.11) help us to compare the diffusion coefficient values. Further, the relaxation and diffusion data for the Drug-IL mixture at different temperatures are presented in Table (4.4 and 4.5).

4.8 Conclusion and Future directions

Nuclear Magnetic Resonance (NMR) spectroscopy is a versatile technique that has contributed a lot in determining the structure of various biological and chemical species. Another important function of NMR spectroscopy is that it provides highly accurate kinetic and dynamics information for the complex liquid system. The applicability of NMR spectroscopy in the drug-IL binding and pharma industry has significantly grown in recent years. Here, NMR spectroscopy is utilized to study the solvation mechanism or dynamics of 5-Furacil in [BMIM] Br. This study focuses on the investigation of the hydrogen-bonding interactions between 5-Furacil and IL, using the combined application of ^{19}F, ^{1}H NMR, and $^{1}H-^{1}H$ NOESY NMR spectroscopy along with DFT calculations using Gaussian 09.

The comparison of ^{19}F NMR spectra of pure drug with the drug-IL mixture, as shown in figure (4.4), displays the shifts in the peaks, which suggest that the change in the environment around nuclei has occurred due to mixing of IL in various concentration. We provided the T_1 and T_2 values for pure drug, pure IL, as well as for their mixtures. Slightly lower T_1 and T_2 values for drug-IL mixtures show that the dynamics or say tumbling of the molecules has decreased. Also, ^{1}H and ^{19}F plots of ln(I/Io) Vs. Time delay for relaxation time and ln(I/Io) Vs. g^2 for diffusion data were provided that helps us to compare the T_1, T_2, and diffusion coefficient of Drug-IL mixtures for different compositions at three different temperatures.

As in the above relaxation and diffusion figures, we can see that pure drug and IL has the highest slope, so as their relaxation times and diffusion coefficient, after mixing of drug-IL, these values start decreasing. Here lowering in relaxation values indicates a lack of freedom in molecular tumbling, and reduced diffusion coefficient can be an indication of an increase in molecular structure size. Both of these indications can be considered as proof of the existence of binding between drug and IL.

Moreover, based on the above relaxation and diffusion data combined with the DFT calculations and $^{1}H-^{1}H$ NOESY NMR, we can say that the proposed dissolution mechanism is reliable to some extent. However, we still need to do another different set of NMR experiments to show more confidence in the findings of our study.

In summary, Br^- anion seems to bind to the hydrogen atoms of N1−H and N2−H (figure 4.2) groups of 5-Furacil. In contrast, the most acidic/labile hydrogen atom (H7) of the bulky $[BMIM]^+$ cation prefers to bind to the carbonyl groups' oxygen atoms uracil, and with the increase of the available number of cations, it also shows weak binding with Fluorine nuclei of the drug (5-FUracil).

Topspin Commands

Command Function

- wrpa To copy the experiment at desired location.
- i To copy the experiment at adjacent position.
- edc To create a directory.
- rsh To read the shim file.
- rga To set receiver gain.
- atma To tune and match automatically.
- atmm To tune and match manually.
- getprosol To set the default values in the experiment.
- pulsecal To calibrate pulse length automatically.
- zg To start acquisition.
- efp To Perform fourier processing.
- apk Automatic phase correction.
- abs Automatic base line correction.

Bibliography

1 Ernst, R. R., G. Bodenhausen, and A. Wokaun. Principles of Nuclear Magnetic Resonance in One and Two Dimensions. Clarendon Press, Oxford. 1987.

2 Derome, A. Modern NMR Techniques for Chemistry Research. Pergamon Press Press, Oxford. 1987.

3 http://library.tedankara.k12.tr/carey/ch13-nmr-1.html

4 chem. latech. Nmr spectroscopy - theory. http://www.chem.latech.edu/ 7Eupali/chem281/ 281lab/NMR/NMRtheory.htm.

5 H. Gu¨nther. NMR spectroscopy: basic principles, concepts, and applications in chemistry. Wiley, 1995.

6 J. Keeler. Understanding NMR Spectroscopy. Wiley, 2005.

7 Abragam, A. Principles of Nuclear Magnetism. Oxford University Press, Oxford. 1961.

8 T.L. James Fundamentals of NMR Department of Pharmaceutical Chemistry, University of California (1998), pp. 1-31

9 P. Hore, J. Jones, and S. Wimperis. NMR: The Toolkit. Ocp Series. Oxford University Press, 2000.

10 S. Pascal. NMR Primer: An HSQC-based Approach with Vector Animations. IM Publications, 2008.

11 D.C. Apperley, A.F. Markwell, I. Frantsuzov, A.J. Ilott, R.K. Harris, P. Hodgkinson, NMR characterisation of dynamics in solvates and desolvates of formoterol fumarate, Phys. Chem. Chem. Phys. 15 (2013) 6422–6430.

12 I. Bertini, C. Luchinat, G. Parigi, Solution NMR of Paramagnetic Molecules, Elsevier, Amsterdam, 2001.

13 R. DuttaMajumadar, M. Gerken, P. Hazendonk. A Nuclear magnetic resonance spectroscopic investigation of the molecular structure and aggregation behaviour behavior of asphaltenes, 2005

14 https://chem.libretexts.org/Bookshelves/Physical_and_Theoretical_Chemistry_Textbook_Maps/Supplemental_Modules_(Physical_and_Theoretical_Chemistry)/Spectroscopy/MagneticResonance_Spectroscopies/Nuclear_Magnetic_Resonance/NMRTheory/Relaxation/Spin_Lattice_Relaxation

15 Darstellung der T1-Relaxation über die Zeit.Quellehttps://mrimaster.com/ physics%20intro. html

16 http://u-of-o-nmr-facility.blogspot.com/2010/02/cpmg-to-enhance-sharp-lines.html

17 https://images.app.goo.gl/DT2SmX2VWGfVgPW89

18 P. Green. Kinetics, Transport, and Structure in Hard and Soft Materials. Taylor & Francis, 2005.

19 K. F. Morris and C. S. Johnson. Diffusion-ordered two-dimensional nuclear magnetic resonance spectroscopy. Journal of the American Chemical Society, 114(8):3139–3141, 1992.

20 W. Price and W. Price. NMR Studies of Translational Motion: Principles and Applications. Cambridge Molecular Science. Cambridge University Press, 2009.

21 W. Price and W. Price. NMR Studies of Translational Motion: Principles and Applications. Cambridge Molecular Science. Cambridge University Press, 2009.

22 C. Tanford, Physical Chemistry of Macromolecules, Wiley, New York, 1961.

23 Y. J. Weitsman. 2.11 - effects of fluids on polymeric compositesa review. In A. Kelly and C. Zweben, editors, Comprehensive Composite Materials, pages 369 – 401. Pergamon, Oxford, 2000.

24 Science direct. Fick's law - an overview — sciencedirect topics. https://www. sciencedirect.com/topics/engineering/ficks-law.

25 D. Sinnaeve. Pfg sequence. http://DavySinnaeveet.al.

26 M. I. Hrovat and C. G. Wade. Nmr pulsed-gradient diffusion measurements. i. spin-echo stability and gradient calibration. Journal of Magnetic Resonance (1969), 44(1):62 – 75, 1981.

27 Heidelberger, C.; Chaudhuri, N.; Danenberg, P. Fluorinated pyrimidines, a new class of tumour-inhibitory compounds. *Nature* **1957**, *179*, 663– 666

28 Focaccetti, C.; Bruno, A.; Magnani, E.; Bartolini, D.; Principi, E.; Dallaglio, K.; Bucci, E. O.; Finzi, G.; Sessa, F.; Noonan, D. M.Effects of 5-fluorouracil on morphology, cell cycle, proliferation, apoptosis, autophagy and ROS production in endothelial cells and cardiomyocytes. *PLoS One* **2015**, *10*, 1– 25,

29 El-Sayyad, H. I.; Ismail, M. F.; Shalaby, F. M.; Abou-El-Magd, R. F.; Gaur, R. L.; Fernando, A.; Raj, M. H.; Ouhtit, A. Histopathological effects of cisplatin, doxorubicin and 5-flurouracil (5-FU) on the liver of male albino rats. *Int. J. Biol. Sci.* **2009**, *5*, 466– 473

30 Longley, D. B.; Harkin, D. P.; Johnston, P. G. 5-Fluorouracil: Mechanism of Action and Clinical Strategies. *Nat. Rev. Cancer* **2003**, *3*, 330– 338

31 Estroff, L. A.; Hamilton, A. D. Water Gelation by Small Organic Molecules. *Chem. Rev.* **2004**, *104*, 1201– 1217

32 Xu, J. F.; Niu, L. Y.; Chen, Y. Z.; Wu, L. Z.; Tung, C. H.; Yang, Q. Z. Hydrogen Bonding Directed Self-Assembly of Small-Molecule Amphiphiles in Water. *Org. Lett.* **2014**, *16*, 4016– 4019

33 Chintala, L.; Vaka, S.; Baranda, J.; Williamson, S. K. Capecitabine versus 5-fluorouracil in colorectal cancer: where are we now?.*Oncol. Rev.* **2011**, *5*, 129– 150

34 Advani, P. P.; Fakih, M. G. 5-FU-induced hyperammonemic encephalopathy in a case of metastatic rectal adenocarcinoid successfully rechallenged with the fluoropyrimidine analog, capecitabine. *Anticancer Res.* **2011**, *31*, 335– 338

35 Gaillon, L.; Siriex-Plenet, J.; Letellier, P. J. *Solution Chem.* **2004**, *33,* 1333.

36 Sirieix-Plenet, J.; Gaillon, L.; Letellier, P. Talanta 2004, 63, 979.

37 Goodchild, I.; Collier, L.; Millar, S. L.; Prokes, I.; Lord, J. C. D.; Butts, C. D.; Bower, J.; Webster, J. P. R.; Heenan, R. K. J. Colloid Interface Sci. 2007, 307, 455.

38 H.Tsuchiya, M.Imanari, S.Ishihara, M.Nakakoshi, K.Nishikawa, H.Seki and M.Tashiro japn. Soc. Chem. 2008, 24, 1369

39 M. R. Prausnitz, R. Langer, *Nat. Biotechnol.* 2008, **26**, 1261.

40 C. R. Harding, *Dermatol. Ther.* 2004, **17**, 6.

41 N. Adawiyah, M. Moniruzzaman, S. Hawatulaila, MGoto, *MedChemComm* 2016, **7**, 1881.

42 A. Banerjee, K. Ibsen, T. Brown, R. Chen, C. Agatemor, S. Mitragotri, *Proc. Natl. Acad. Sci. USA* 2018, **115**, 7296.

43 R. Notman, W. K. den Otter, M. G. Noro, W. J. Briels, J. Anwar, *Biophys. J.* 2007, **93**, 2056.

44 R. Gupta, B. S. Dwadasi, B. Rai, S. Mitragotri, *Sci. Rep.* 2019, **9**, 1456.